AD-A119 707 B-K DYNAMICS INC ROCKVILLE MD F/G 9/1
GYROTRON GUN STUDY REPORT,(U)
SEP 81 J M BAIRD, A C ATTARD N000173-79-C-0132
UNCLASSIFIED TR-3-476 NL

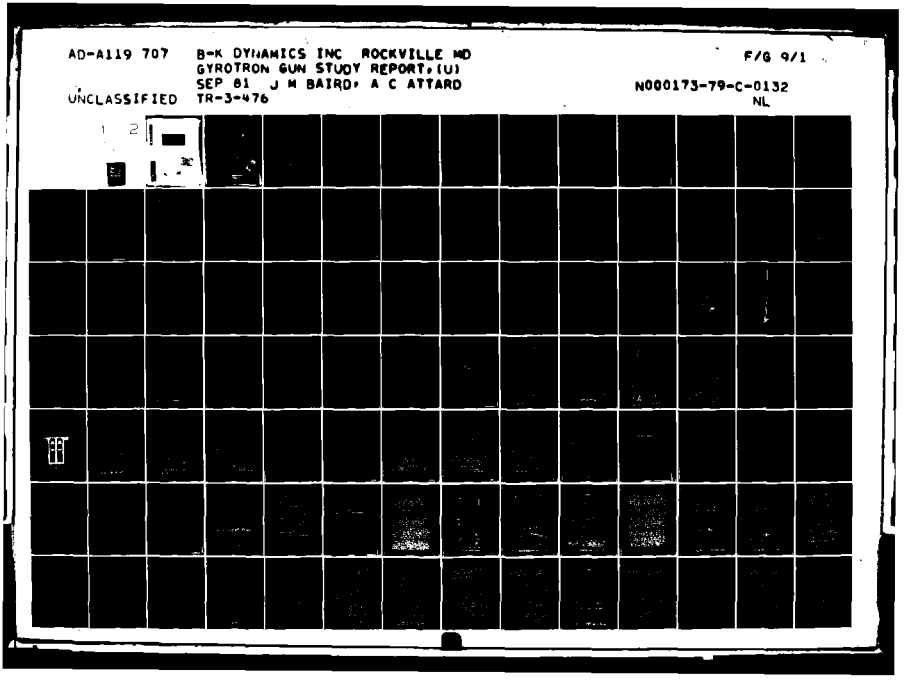

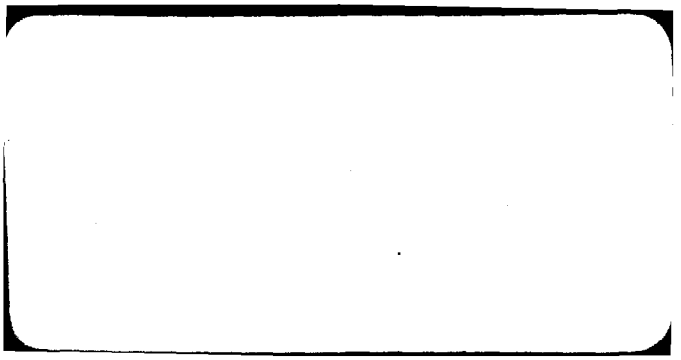

TR-3-476

GYROTRON GUN STUDY REPORT

18 September 1981

Prepared by:

J. Mark Baird,

Anthony C. Attard

B-K Dynamics, Inc.
15825 Shady Grove Road
Rockville, Maryland 20850

Prepared for:

The Naval Research Laboratory
Under Contract N000173-79-C-0132

TR-3-476

GYROTRON GUN STUDY REPORT

18 September 1981

Prepared by:

J. Mark Baird,

Anthony C. Attard

B-K Dynamics, Inc.
15825 Shady Grove Road
Rockville, Maryland 20850

Prepared for:

The Naval Research Laboratory
Under Contract N000173-79-C-0132

ACKNOWLEDGEMENTS

This work was jointly sponsored by the Electronics and Plasma Physics Divisions of the Naval Research Laboratory. The authors are very grateful for the cooperation and assistance extended by the staffs of these Divisions and in particular would like to thank Drs. N. Vanderplaats and V. Granatstein for many helpful discussions throughout the course of this work. Computer time for the simulations required in this work was provided by the NRL computer facility.

TABLE OF CONTENTS

List of Figures

List of Figures

List of Tables

SECTION I

GYROTRON GUN STUDY PROGRAM

GYROTRON GUN STUDY PROGRAM

I. INTRODUCTION

This final report describes the results of a gyrotron gun study performed by B-K Dynamics for the Naval Research Laboratory under Contract No. N00173-79-C-0312.

The purpose of the program was to explore new gyrotron gun configurations and to design a low velocity spread replacement gun for the NRL 35 GHz gyro-TWT. The specific beam forming techniques which were studied were magnetic field reversal, transverse magnetic field kicker, and single anode (diode-like) Magnetron Injection Guns (MIGs). This report contains a summary of our work in each of these areas as well as a description of the new MIG design for the gyro-TWT.

Gyrotron oscillators and amplifiers require an entirely different type of electron gun design than those normally used in conventional tube designs. The ideal beam must not only have the proper geometry to maximize the rf interaction with the selected waveguide circuit mode, but also, for maximum efficiency, there are two additional requirements: 1) the transverse velocity of the electrons must exceed the longitudinal velocity by a typical factor of 1.5 to 2 (intermixed helical electron trajectories are allowed); and 2) the spread in the longitudinal velocities must be small (on the order of 10-20% for oscillators, 2-5% for amplifiers).

Several methods for producing gyrotron beams have been investigated, and most likely different approaches will be necessary for differing power levels and velocity spread requirements.

1.1 HISTORY OF GYROTRON GUN DESIGN

Historically, several beam formation schemes were proposed and tried by researchers investigating cyclotron wave interactions in the 1960's. In the U.S., Chow and Pantell (1960) first used a magnetically shielded, off-axis Pierce gun to produce a beam with helical electron trajectories. They also used a ring cathode version of the same approach. Wingerson (1961) proposed the use of a bifilar helix to act as a transverse parametric pump on an axial pencil beam with subsequent magnetic compression to achieve high transverse velocities. Hirshfield, et al. (1965) used this technique in some of the first truly definitive gyrotron experiments.

Both of these beam generation schemes, as well as a related tilted-Pierce-gun scheme described by Korolev and Kurin (U.S.S.R. 1970), are based on magnetically-shielded, space-charge limited guns with the subsequent addition of the transverse velocity component in the beam. There has been a renewed interest recently in this general approach due to the desire to find ways to utilize standard gun technology and to achieve lower longitudinal velocity spreads.*

The high power gyrotron successes to date, however, have been achieved with modified magnetron injection guns (MIGs). These guns were first tried experimentally in the U.S. by Dickerson and Johnson (1964) and were used by Schriever and Johnson (1966) to produce a relatively high power cyclotron wave BWO. Gapanov, et al. (1965) first reported the use of this type gun in the Soviet Union and subsequent work by Soviet researchers during the last decade has been extensive (see Appendix A).

---

* Non-MIG approaches to gyrotron guns are actively being pursued in the USA at NRL, Yale University, Varian and Raytheon.

1.2 CURRENT GUN DESIGN APPROACHES AND PROBLEMS

Typical design practice is to generate hollow electron beams using temperature limited MIGs in which the transverse velocities are deliberately enhanced and controlled. (This design approach differs sharply from the early space-charge limited MIGs described by Kino and Taylor (1962) and Dryden (1962) in which one of the design goals was the elimination of transverse velocities.) Control of the longitudinal velocity spread in the beam is one of the difficult problems in the design of gyrotron guns.

The three primary sources of velocity spread (both transverse and longitudinal) in a MIG-type, temperature-limited gyrotron gun are: 1) electron ray optics, 2) cathode thermal velocities, and 3) cathode roughness. In the ray optics case, longitudinal velocity spread arises from the spatial differences in the electron ray trajectories which originate at different points along the cathode. This includes trajectory space-charge effects in the beam. In the other two cases, velocity spread is the result of a spread in the initial velocities at the cathode.

1.3 REPORT OUTLINE

The order of presentation in this report is as follows. Section II gives a description of a new set of adiabatic MIG design trade-off equations which can be used with highly tilted cathodes to obtain a starting point for computer simulation and optimization. Section III then provides the details of the new single anode MIG design for the NRL 35 GHz gyro-TWT. Section IV gives the results of magnetic field reversal studies and some new analysis on a

transverse magnetic field kicker scheme which looks very promising for low velocity spread, variable velocity ratio experiments. Finally, Section V presents conclusions and recommendations resulting from this gun design study.

Three appendices are included which give: (A) a very illuminating overview of Soviet MIG research in the past fifteen years, (B) the derivation and application of gun design equations related to conservation of angular momentum, and (C) a detailed discussion of the derivation of the gun design trade-off equations in Section II.

SECTION II

EXPANDED THEORY OF MAGNETRON INJECTION GUNS (MIGS) FOR GYROTRON APPLICATIONS

II. EXPANDED THEORY OF MAGNETRON INJECTION GUNS (MIGS) FOR GYROTON APPLICATIONS

Previous reports* have dealt with many aspects of the theory of adiabatic MIG design. In this report, we present an expanded view of this subject with two important additions. The first is an approximate theory which permits design trade-off calculations on guns with large cathode tilt angles. The second is the addition of equations which give an estimate of the velocity spreading in the beam due to cathode temperature and surface roughness.

By way of introduction, we reemphasize here that present-day gyrotron gun design procedure relies heavily on accurate computer simulation of the helical trajectories in the relative complex electron beam. The design optimization procedure is one of synthesis-by-computer-analysis, i.e., an iterative "cut and try" approach in which one hopes to be able to converge from an initial "test" design to a final optimized design which meets desired performance specifications. The computer simulations themselves, however, give very little insight into the basic physical principles of MIG design. Lack of a clear phenomenological model can result in slow convergence and great inefficiency and frustration in the design process unless one is able to determine a suitable initial gun design from which optimization can proceed via simulation. The adiabatic design trade-off equations developed here provide a physical basis for selecting an initial gun design provided the resulting beam flow is reasonably adiabatic They are derived from the basic equations of motion of spiraling electrons in static electric and magnetic fields under the assumption of adiabatic beam flow from the cathode to the rf interaction region.

---

* Baird and Amboss, 1978, and Baird and Attard, 1981

In practice, it has been found that the adiabatic assumption is sufficiently justified for most gun designs to provide a reasonable starting point for computer simulations. The final optimal gun design resulting from the simulation -- which includes both adiabatic and non-adiabatic processes -- may or may not be adiabatic. In some cases it may even be advantageous to use non-adiabatic effects to enhance transverse beam velocities. At the present stage of theoretical development, however, we know of no comprehensive analytical theory which permits direct design using weakly non-adiabatic effects, and therefore those effects are not included in the design trade-off equations presented here.

Another factor which can also have significant effects on the final MIG design, and which is also not included explicitly in the design trade-off equations, is space charge. Although the equations do provide an estimate of when space charge effects become serious, space charge effects are most easily determined by accurate computer simulation.

The remainder of this Section gives a discussion of the background and use of the design trade-off equations, which are summarized in Table I(a) with the definition of terms in Table I(b). A more comprehensive derivation of the equations is given in Appendices B and C.

2.1 DESIGN TRADE-OFF EQUATIONS

When adiabatic beam flow is assumed throughout the beamforming system (i.e., the magnetic moment of the spiraling electrons is conserved), it has been found that most of the design parameters in the cathode region of the gun can be written as a simple power function of the cathode radius times a

TABLE Ia

Design Trade-off Equations for Adiabatic Gyrotron MIGs

1. $B_{zc} r_c^2 = B_o(b_o^2 - a_o^2)$ $\equiv C_B$

2. $E_c r_c^3 = \dfrac{\gamma_o v_{\perp o} C_B^{3/2}}{B_o^{1/2}\cos(\phi_c+\theta_B)}$ $\equiv C_E$

3. $d\, r_c^{-1} = \dfrac{\zeta a_o}{(b_o^2 - a_o^2)^{1/2}}$ $\equiv C_d$

4. $V_a r_c^2 = \dfrac{C_E \ln(1+C_d\cos\phi_c)}{\cos\phi_c}$ $\equiv C_V$

5. $\left(\dfrac{I_o}{I_\perp}\right) r_c^{-5} = \dfrac{2\pi J_c(1+C_d\cos\phi_c)\beta^2}{14.66(10^{-6})C_V^{3/2}\cos^2\phi_c}$ $\equiv C_L$

6. $\left(\dfrac{\Delta v_\perp}{v_\perp}\right)_T r_c^{-1} = \pm\left[\dfrac{C_B\left(kT_c/m_o\right)^{1/2}}{C_E\cos\left(\phi_c + \theta_B\right)}\right]$ $\equiv \pm C_T$

7. $\left(\dfrac{\Delta v_\perp}{v_\perp}\right)_R r_c^{1/2} = \pm\left[\dfrac{0.4\, C_B\sqrt{2\eta R}}{C_E^{1/2}\cos(\phi_c+\theta_B)}\right]$ $\equiv \pm C_R$

8a. $I_o r_c^{-2} = 2\pi\left(\dfrac{\ell_s}{r_c}\right) J_c$ $\equiv C_I$

8b. $\left(\dfrac{\ell_s}{r_c}\right) r_c^2 = \dfrac{I_o}{2\pi J_c}$ $\equiv C_\ell$

alternative equations

TABLE Ib

Definition of Table Ia Variables (mks units)

r_c	=	Mean cathode radius
B_{zc}	=	Longitudinal magnetic field at the cathode
B_o	=	Magnetic field in rf interaction region
b_o	=	Final beam guiding center radius (central electrons)
a_o	=	Final cyclotron radius of electrons = $v_{\perp o}/\omega_c$
E_c	=	Surface electric field at midpoint of cathode
γ_o	=	Final beam relativistic mass ratio = m/m_o
$v_{\perp o}$	=	Final beam transverse velocity
ϕ_c	=	Cathode angle with respect to axis (positive)
θ_B	=	Magnetic field angle WRT axis at cathode (negative for converging field)
d	=	Cathode-anode spacing measured normal to cathode
ζ	=	Number of Larmour radii across cathode-anode gap (can be adjusted for any desired anode voltage)
V_a	=	First anode voltage
I_o	=	Total beam current
(I_o/I_L)	=	Ratio of beam current to space-charge limited Langmuir current
J_c	=	Cathode surface current density
β^2	=	Cylindrical diode geometry function (tabulated in Appendix C, Table CII). The argument of this function is $(1 + C_d \cos\phi_c)$.
$(\Delta v_\perp/v_\perp)_T$	=	Standard deviation of transverse velocity spread in beam due to initial thermal velocities
kT_c/m_o	=	Boltzmann's constant x cathode temperature/electron mass
$(\Delta v_\perp/v_\perp)_R$	=	Standard deviation of transverse velocity spread in beam due to cathode roughness
R	=	Characteristic roughness height of cathode (radius of hemispherical bump on cathode surface)
η	=	$\lvert e\rvert/m$ = charge to mass ratio of electrons.
(ℓ_s/r_c)	=	Ratio of slant length of cathode to mean radius

constant which depends only on selected design parameters. Once the constants are calculated, therefore, a system of equations results which permits a rapid determination of the alternative adiabatic gun configurations which will produce the desired electron beam. The equations quickly indicate the ranges of cathode radius r_c which, under adiabatic conditions, will produce acceptable design values.

The primary physical limitations that constrain permissible values of r_c have been found to result from equations 2 and 5 in Table I. Equation 2 gives a lower bound on r_c due to the fact that the maximum permissible electric field at the cathode, $E_c(max)$, must typically remain below 80 to 100 kV/cm) to prevent arcing in the gun. Thus

$$r_c(min) = [C_E/E_c(max)]^{1/3}$$

Equation 5, on the other hand, gives a very sharply limited upper bound $r_c(max)$ depending on the maximum acceptable value of (I_o/I_L). Thus

$$r_{c(max)} = [(I_o/I_L)_{max}/C_L]^{1/5}$$

The 1/5 power exponent assures that $r_c(max)$ is relatively insensitive to most numerical changes in the initial design parameters. Thus, it is of little consequence that: a) the maximum value of C_L is only an estimate; and b) the maximum permissible value of (I_o/I_L) is somewhat a matter of intuition until computer simulations of the gun are carried out. The fixed upper limit on the cathode size becomes a severe problem for temperature-limited MIGs in the high power, high voltage regime because $r_c(min)$ can exceed $r_c(max)$ in which case no design region exists.

With these preliminary observations on the overall use of the equations, we now focus on each equation individually to describe its meaning and limitations.

1. Magnetic Field at the Cathode, B_c

Of all the equations in Table I, Equation 1

$$B_{zc} r_c^2 = B_o(b_o^2 - a_o^2) \equiv C_B \qquad (1)$$

is unique because it is the one major equation in the table which does not rely on the adiabatic assumption, and therefore has fundamental importance in a wide variety of gyrotron beam synthesis work. The equation comes from the conservation of angular momentum and to our knowledge was first published in this form* by Baird and Amboss (1978). Appendix B of this report gives a new derivation of this equation which provides additional insight into its meaning and applications. The derivation relies only on the assumptions that the static electric and magnetic fields in the beam forming system are azimuthally symmetric, that thermal velocities can be neglected, and that the magnetic field can be represented by

$$\vec{B} = \nabla \times \vec{A} = \left(\frac{-r}{2}\frac{dB_z}{dz}, B_z\right) \equiv \left(B_r, B_z\right)$$

Although this latter approximation is usually thought of as an axial one in which $B_r \ll B_z$, it can be shown (see Appendix B) that the equation also applies in the limit where B_z has a sharp step functioning variation corresponding to a narrow cusp function (or delta function) in B_r. Equation 1, therefore,

* The initial publication contained a factor of γ which was in error.

is valid for a wide range of gyrotron gun problems including the non-adiabatic cases where stepped magnetic fields are used to generate transverse velocity in the beam.

For example, if $B_{zc} = -B_{zo}$ and $r_c = a_o$, Equation 1 gives the field reversal conditions under which a thin annular beam with no transverse velocity becomes a hollow rotating beam which is spiraling uniformly about the z axis. Also note that if $B_{zc} = o$ (i.e., a magnetically shielded cathode with a subsequent application of a magnetic field), then Equation 1 requires $b_o = a_o$ so that all of the cyclotron orbits pass through the $r = o$ axis, i.e., z axis. This is one mechanism which produces scalloping in conventional focused beams.

For ring cathodes in a magnetic field such as those used in gyrotron MIGs, Equation 1 gives an extremely simple and important design relationship between cathode radius and cathode magnetic field. This equation holds for cylindrically symmetric beam forming systems regardless of beam acceleration and compression, and regardless of non-adiabatic effects. Note that the relationship between r_c and B_{zc} is fixed once the desired beam geometry and magnetic field in the rf interaction region are fixed. Thus Equation 1 can be used as a design trade-off relationship in determining the size of the cathode required. The right hand side of Equation 1 is designated as the design constant C_B as shown.

It should be noted here that even though the correct values for B_{zc} and r_c are utilized in a given gun design, Equation 1 does not guarantee that the desired values of b_o and a_o will be attained. Once B_{zc}, r_c, and B_o are fixed, there is a linear relationship between b_o and a_o which satisfies the equation. The exact values of b_o and a_o achieved will depend on how the beam is formed at the cathode and transmitted to the interaction region.

Equation 1 does guarantee, however, that if the wrong values of B_{zc} and r_c are used in a gun design, then the desired values of b_o and a_o will not be simultaneously achievable.

In practice, if Equation 1 is satisfied and if the diameter is sufficiently large that $b_o^2 >> a_o^2$, then the desired value of b_o will be attained to a close approximation regardless of the value of a_o. However, the velocity ratio ($\alpha = v_\perp/v_z$) which depends on the value of a_o, can have a wide variation. Control of the velocity ratio and, in particular, the spread in the velocities, $(\Delta v/v)$, is the principal challenge in gyrotron gun design.

2. Electric Field at the Cathode, E_c

Equation 2 in Table I

$$E_c r_c^3 = \frac{\gamma_o v_{\perp o} C_B^{3/2}}{B_o^{1/2}\cos(\phi_c+\theta_B)} \equiv C_E \qquad (2)$$

is the direct result of the application of the adiabatic invariance of the magnetic moment. If one specifies that the initial transverse velocity at the cathoded is given by $E_c \sin\theta_{EB}/B_c$, which comes from $(\vec{E} \times \vec{B})/B^2$, then the equation shown results from equating the value of the magnetic moment at the cathode to its value in the rf interaction region.

In equation 2, we have used the constant C_B (Equation 1) to eliminate B_c to get a trade-off relationship between E_c and r_c. The angles shown in the equation are ϕ_c which is the positive angle between the cathode and the axis (i.e., the cathode tilt angle), and the magnetic field angle θ_B (assumed small) which is the signed angle between the magnetic flux at the cathode and the gun axis. In this formulation, a negative angle represents a magnetic field converging toward the rf interaction region.

Equation 2 shows that for a specified beam geometry (C_E = constant), that the effect of increasing the cathode radius is a rapid reduction in the required electric field at the cathode ($E_c \sim r_c^{-3}$). As will be seen, this strong functional relationship gives the primary contribution to the absolute upper limit of r_c which was previously described and which becomes evident in Equation 5. Equation 2 is the basis for the lower bound on the cathode radius. If we insert the maximum permissible cathode field E_{cmax} into the equation and solve for the cathode radius, the result is

$$r_c(\text{Min}) = \left[C_E/E_c(\text{Max})\right]^{1/3}$$

Any attempt to reduce the cathode radius below this value will result in excessive cathode fields. Alternately, once the cathode radius if fixed, any attempt to reduce the electric field at the cathode (for example by lowering the first anode voltage) will result in a low value for the transverse velocity in the interaction region. The exception to the above constraints is the case of a non-adiabatic gun in which the beam transverse velocity is changed (either increased or decreased with respect to the adiabatic value) as the beam passes through the non-adiabatic region(s) of the gun. As previously noted, such non-adiabatic design cases do exist and need to be further explored in order to find a systematic method for taking advantage of these effects to permit greater flexibility in design than allowed by the adiabatic design conditions.

3. Anode-Cathode Gap Spacing, d

Equation 3 in Table I relates the anode-cathode gap spacing d to the design geometry of the beam through the use of an arbitrary design factor ζ.

$$d\, r_c^{-1} = \frac{\zeta a_o}{(b_o^2 - a_o^2)^{1/2}} \equiv C_d \qquad (3)$$

Basically, this equation arises from the recognition that the gap spacing must be at least twice the radius of the cyclotron radius a_c at the cathode, since 2 a_c is approximately the height that the beam rises above the cathode, (estimated from plannar geometry relationships). We have therefore elected to make the gap spacing proportional to the cyclotron radius at the cathode with ζ as the proportionality constant selected by the designer ($d = \zeta a_c$). When this is evaluated using $a_c = v_{\perp c}/\omega_c$ and Equations 1 and 2 are used to eliminate B_c and E_c, the result is a simple scaling of the anode-cathode gap in proportion to the cathode radius.

In practice, one can use the arbitrary design parameter ζ to adjust the voltage on the first anode to any desired level. Practical values of ζ usually lie between 3 and 10 although larger values can occur for single anode designs in which the full beam voltage is applied to the first anode.

4. <u>First Anode Voltage, V_a</u>

In general MIG designs utilize conically tapered cathode and electrode surfaces. The conical shape provides the axial component of the electric field which accelerates the beam out of the cathode region of the gun. When the cathode "tilt" angle (ϕ_c) with respect to the z axis is small, it is sufficient to use coaxial electrode theory to determine the anode radius and voltage which provides the desired electric field at the cathode. There are other considerations having to do with velocity spread, however, which makes it desirable to use larger cathode tilt angles. Tsimring (1977) and Manuilov and Tsimring (1979) have shown that by tilting the cathode to

a sufficiently large angle, laminar flow behavior can be achieved in gyrotron guns. Laminar flow has the important effect of causing cancellation of velocity spreading forces due to space charge in the highly rippled beam formed by the MIG. Thus, cathode tilt angles of 15° to 45° can be beneficial in high space-charge gun designs. For the designer, this creates a new problem of estimating the anode voltage which will provide the required electric field at the cathode of the highly tilted conical electrode system.

To assist in estimating the anode voltage, we have put some effort into devising a method for including the effects of the cathode tilt angle into the MIG design trade-off equations. The method discovered is surprisingly simple, and, to date, has given results which are within a few percent of values taken from computer simulations. Because the equations involved are asymptotically correct at cathode angles of 0 and 90 degrees, we believe that the resulting design trade-off equations can be used effectively to synthesize first order MIG designs (at any cathode tilt angle) which are suitable for the purpose of initializing a design simulation.

The solution to the problem was found by assuming that the electric field at any point on the cathode is primarily determined by the surface curvature of the cathode and by the approximate spacing to the nearest point on the anode (assumed to occur at a point normal to the cathode surface). With some effort it is possible to show that the radius of curvature on the surface of a cone (measured with respect to the surface normal) is simply the distance from the surface of the cone to the axis, as measured along the direction normal to the surface. Thus, the <u>effective</u> radius of curvature of a cathode with a tilt angle ϕ_c is given simply by $r_c' = r_c/\cos\phi_c$ as shown in Figure 1.

We continue the analysis by assuming that the first anode is formed by an identical coaxial cone which is shifted along the axis sufficiently to make the separation between the cathode and anode surface equal to d (again in the direction normal to the cathode surface). Then, based on the original assumption, the voltage on this anode is given approximately by coaxial field theory in which the effective curvature of the cathode r_c' is used as the inner radius and $(r_c' + d)$ as the outer radius of the electrodes.

The results of this procedure have proven to be accurate within a few percent in predicting the relationship between the anode V_a and the cathode electric field E_c in computer simulations of MIGs. The comparison has been made at several cathode angles between 30 and 70 degrees and at various cathode radii. Further evidence of the validity of the approximation over a wide range of angles is the fact (noted above) that in the two limits $\phi_c = 0$ and $\phi_c = 90$ degrees, the equations relating voltage and electric field approach the respective limiting equations for uniform coaxial electrodes and planar electrodes.

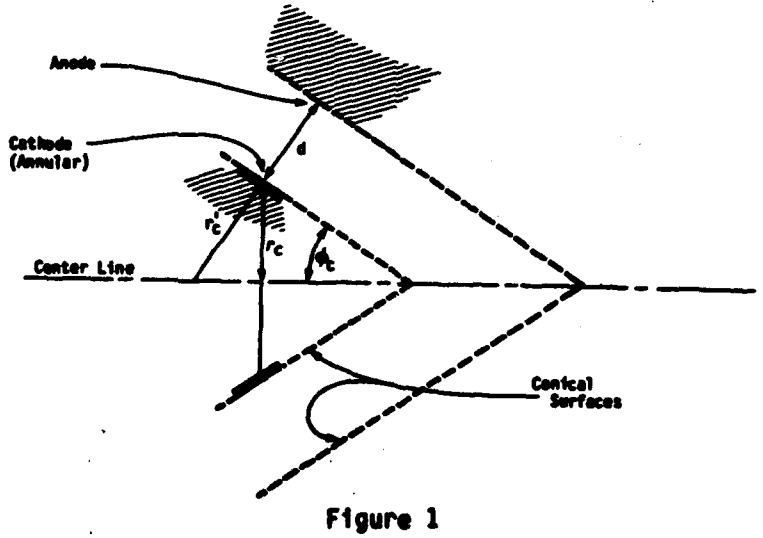

Figure 1

Model for Effective Cathode Radius r_c' and Anode Spacing d for MIGS with Large Cathode Angle Tilts ϕ_c

The resulting design trade-off equation for first anode voltage V_a is given by

$$V_a r_c^2 = \frac{C_E \, \ell n(1+C_d \cos\phi_c)}{\cos\phi_c} \equiv C_V \qquad (4)$$

To obtain this equation, we have used the two radii r_c and $(r_c + d)$ in the coaxial equation relating E_c and V_a. We then used Equations 2 and 3 to eliminate E_c and d and obtain the design trade-off equation shown.

In MIG design, it is not necessary to make the first anode voltage V_a equal to the final beam voltage. Many gyrotron MIG designs use two anodes so that V_a is at some intermediate voltage. In this case, the first anode can be used as a control electrode to trim the beam performance or to modulate the beam. The minimum design voltage which can be used on the first anode is that which begins to cause beam interception because the spacing is too small.

When V_a is less than the final beam voltage V_o, a second acceleration gap must be designed into the gun. This second gap can sometimes produce serious non-adiabatic effects in the beam flow and cause velocity spread problems. These problems are most likely to occur when V_a is much lower than V_o or when strong lens effects are associated with the second acceleration gap. The best way to determine the magnitude of these effects is through computer simulation.

5. Beam Current as a Fraction of the Limiting Langmuir Current (I_o/I_L)

Equation 5 in Table I is basically intended to provide a measure of the space-charge effects in a MIG design. The trade-off equation provides an estimate of the temperature limited beam current I_o as a fraction of the

space-charge limited current I_L which would exist in the absence of the magnetic field. The quantity (I_0/I_L) is given by

$$\left(\frac{I_o}{I_L}\right) r_c^{-5} = \frac{2\pi J_c (1+C_d \cos\phi_c)\beta^2}{14.66(10^{-6})C_V^{3/2}\cos^2\phi_c} \equiv C_L \qquad (5)$$

where the function β^2 (described in Appendix C, Table CII) has the argument $(1+C_d \cos\phi_c)$. To obtain this equation, we have used coaxial diode theory in which we have again substituted the values of r_c' and $(r_c' + d)$ as the inner and outer radii. We have been able to show (see Appendix C) that when the cathode tilt angle is increased to 90 degrees that the resulting equation is equivalent to the plannar diode case. It therefore appears probable that the technique given here provides a reasonable estimate for the Langmuir limiting current for all cathode tilt angles, although this has never been verified by computer simulations.

The strong functional dependence $(I_0/I_L) \sim r_c^5$ comes about because I_L varies directly with $V_a^{3/2}$ and approximately inversly with d^2. The result if

$$I_L \sim V_a^{3/2}\, d^{-2} \sim r_c^{-3}\, r_c^{-2} = r_c^{-5}.$$

This strong dependence makes (I_0/I_L) very sensitive to increasing values of r_c and produces a sharply defined practical upper limit for r_c, beyond which severe space change effects are encountered.

At best, the value of (I_0/I_L) obtained from this method is only a rough estimate. This is not only true because the magnetic field is neglected, but also because only a narrow strip cathode is utilized in the gun. Experience has shown, however, that the value obtained by Equation 5 does give a rather effective indicator of the onset of space-charge problems in MIG design.

Once r_c is sufficiently large to make I_o/I_L as large as 10-30%, no further increase is possible without encountering severe space charge problems. As previously noted, we can invert equation 5 to give the maximum r_c as

$$r_c(\text{max}) = \left[(I_o/I_L)\text{max}/C_L\right]^{1/5}$$

Thus $r_c(\text{max})$ is very insensitive to adjustments in the numerical value of $(I_o/I_L)_{max}$. To avoid space-charge problems, therefore, one should select a cathode radius size smaller than $r_c(\text{max})$ if possible.

Two space-charge effects in adiabatic gyrotron MIGs force the maximum permissible beam current to remain well below the space charge limit. The first effect is one which is described by Gol'enberg and Patelim (1973) in which the transverse velocity spread at the output of the gun increases linearly with current. The effect is a direct result of electron trajectories which cross and recross each other due to a low cathode angle. The effect has been measured by Avdoshin, et al. (1973) and shows that beam currents as low as 10 to 20% of I_L can produce excessive velocity spreads. Computer simulations of such beams also demonstrate this effect, (Baird and Amboss, 1978). When a given MIG design uses a high angle cathode and a laminar flow beam within the gun accelerator region, this space-charge effect is greatly reduced.

The second space-charge effect is simply the depression of the electric field at the cathode as the beam current begins to exceed 20 to 30% of the Langmuir limit. Gyrotron MIGs operating at currents approaching 50% I_L and above require an entirely different design approach in which the self-consistent space-charge flow equations are utilized and the gun electrode

geometries which support the beam flow are synthesized in a self consistent manner. As discussed in Appendix A, Manuilov and Tsimring (1979) have described this procedure for temperature-limited gyrotron MIG design. The theory is an extension of that developed by Harker (1960-63) for space-charge limited MIG design. Tsimring (1977) indicates that gyrotron MIG designs have been built and tested in which the electric field at the cathode is depressed (by space charge) to 50% of the field intensity in the absence of space charge. There appears to be no reason why current levels approaching the Langmuir limit cannot be achieved while still maintaining adequate control of velocity spread for many applications. Computer codes which will accomplish this type of gun synthesis are scheduled for development at NRL in FY-82. For the present design trade-off analysis, however, experience thus far has indicated that it is necessary for (I_O/I_L) to remain below 20-30%.

6. Velocity Spread Resulting from Cathode Temperature and Surface Roughness

Equations 6 and 7 from Table I are as follows:

$$\left(\frac{\Delta v_\perp}{v_\perp}\right)_T r_c^{-1} = \pm \left[\frac{C_B \left(kT_c/m_o\right)^{\frac{1}{2}}}{C_E \cos\left(\phi_c + \theta_B\right)}\right] \equiv \pm C_T \qquad (6)$$

$$\left(\frac{\Delta v_\perp}{v_\perp}\right)_R r_c^{1/2} = \pm \left[\frac{0.4\, C_B \sqrt{2nR}}{C_E^{1/2} \cos\left(\phi_c + \theta_B\right)}\right] \equiv \pm C_R \qquad (7)$$

Equations 6 and 7 are derived from equations given by Tsimring (1972) for the initial transverse velocities at the cathode. Equation 6 pertains to the initial transverse velocity arising from the cathode.

temperature and equation 7 is derived from an analysis of transverse velocities resulting from a small hemispherical bump on the cathode surface (approximating surface roughness). Using these initial transverse velocities as $\Delta v_{\perp c}$ and using the value of $v_{\perp c} = E_c \sin\theta_{EB}/B_c$, we formed the ratio $(\Delta v_{\perp c}/v_{\perp c})$ at the cathode. Under adiabatic flow conditions, this ratio is a constant and therefore, these same transverse velocity spread ratios are transmitted into the rf interaction region.

To use equations 6 and 7, one simply evaluates the design constants C_T and C_R; when a suitable value for r_c is determined, the equations give estimates of the transverse velocity spread components resulting from temperature T_c (degrees Kelvin) and cathode roughness R. These velocity spread sources are statistically independent from the velocity spread resulting from electron ray optics $(\Delta v_\perp/v_\perp)_0$ which can be determined from the computer simulations of the beam (including space-charge). Because they are statistically independent, the statistical variances add and the three sources of velocity spread combine as an RMS average to provide the following total standard deviation of perpendicular velocity in the interaction region.

$$(\Delta v_\perp/v_\perp)_{total} = [(\Delta v_\perp/v_\perp)_0^2 + (\Delta v_\perp/v_\perp)_T^2 + (\Delta v_\perp/v_\perp)_R^2]^{1/2}$$

To get the final longitudinal velocity spread one uses the relationship

$$\Delta v_z/v_z = \alpha^2 \, \Delta v_\perp/v_\perp$$

which results from the equation $v_0^2 = v_z^2 + v_\perp^2$ when the total electron velocity v_0 is a constant. The variable α is the average transverse to longitudinal velocity ratio.

7. Cathode Current I_o and Slant Length ℓ_s

Equations 8 in Table I simply state that I_o/J_c = cathode area; the key parameter determining power and current capacity of the gun design and also a key parameter in controlling velocity spread of emitted electrons due to the finite width of the cathode.

$$\left\{ I_o r_c^{-2} = 2\pi\left(\frac{\ell_s}{r_c}\right) J_c \right\} \quad \text{alternative equations} \quad \equiv C_I \tag{8a}$$

$$\left\{ \left(\frac{\ell_s}{r_c}\right) r_c^2 = \frac{I_o}{2\pi J_c} \right\} \quad \text{alternative equations} \quad \equiv C_\ell \tag{8b}$$

give alternate expressions for the relationships among cathode current, I_o, cathode slant length ℓ_s, and cathode surface current density J_c. The cathode radius r_c in this case is assumed to be the mean radius of an annular conical strip cathode. The slant length ℓ_s is the surface width of the annular cathode. We have elected to normalize the slant length of the cathode to the cathode radius so that their relative geometries are preserved in the gun as cathode radius is changed in the design trade-off. Thus, ℓ_s/r_c is treated as a single quantity. This choice may not be the most desirable in some cases (for example when a constant width cathode is desired) but one is free to rewrite equations 8 in alternative forms without effecting the foregoing equations in Table I.

Equation 8(a) is written in a form which allows an estimation of the maximum power achievable in a MIG when the maximum cathode width $(\ell_s/r_c)_{max}$ is

specified. Although large widths permit large currents and power, very wide cathodes also increase velocity spread due to electron ray optics (i.e., large differences in the path trajectories of electrons emanating from different points along ℓ_s). Therefore one usually attempts to keep (ℓ_s/r_c) small, if possible, typically $\lesssim 0.3$. Equation 8(b), alternatively, is useful when one is designing to a specified power level and needs to know the slant width of the cathode which will produce the desired value of beam current. In each case, the desired value of cathode current density is a specified constant of the design.

This concludes the description of the MIG design trade-off equations given in Table I. Additional details on the derivation of the equations are given in Appendices B and C. In the next section we describe the design of a single anode MIG which started with the design trade-off equations and proceeded through computer simulation and optimization to a final design.

SECTION III

DESIGN OF A LOW VELOCITY SPREAD MIG FOR THE NRL 35 GHZ GYRO-TWT

III. DESIGN OF A LOW VELOCITY SPREAD MIG FOR THE NRL 35 GHZ GYRO-TWT

NRL has conducted several experiments on 35 GHz TE_{01} mode gyro-TWT amplifiers over the past four years. Results were reported first by Seftor, et.al. (1979) and most recently by Barnett, et.al. (1979-1981). The efficiencies of these amplifiers have ranged from a few percent to a high of 8%; the shorter, lower gain amplifiers give the best efficiency performance.

All of these experiments utilized the same type MIG gun which was designed by Seftor, Drobot, and Chu, (1979) at NRL. This gun has provided excellent performance in gyronotron oscillators but, thus far, has not performed well in amplifiers. Computer simulations indicate that the Seftor gun has a velocity spread on the order of $\pm$ 8%, but experimental rf results seem to indicate a possibility of up to twice this value. Only a small amount of direct measurement data has as yet been taken on the beam produced by this gun and the results seem to indicate a very complex velocity spread distribution with possibly two velocity components of widely differing velocity spreads.*

In any case, it has become evident in the past two years that a new gun design with a lower velocity spread is needed for gyro-TWT applications. One of the purposes of this gun study program has been to provide such a gun design and we report the results of this work in this section.

The major constraint on the new gun design was that it be a direct replacement for the existing Seftor gun. This will permit several of the gyro-TWT experiments previously performed to be repeated in an effort to document the anticipated efficiency improvements resulting from the use of a lower velocity spread MIG.

---

* Private communication with Dr. Larry Barnett, NRL.

The beam design parameters for the Seftor gun are given in Table II along with the changes/improvements which pertain to the low velocity spread MIG design described in this section.

Table II

Parameters	Seftor Design Values	New Design Values
Beam Voltage	V_o = 70 kV	Same
Current	I_o = 9A	Same
Velocity Ratio	$v_\perp/v_z$ = 1.5	Same
Guiding Center Radius	b_o = 0.252 cm	Same
Larmor Radius	a_o = 0.052 cm	Same
Interaction Mag. Field	B_o = 12.96 kG	Same
Cathode Mag. Field	B_c = 1860 G	Same
Cathode Current Density	J_c = 4 A/cm^2	10 A/cm^2
Cathode Angle	ϕ_c = 10°	40°
First Anode Voltage	V_a = 35 kV	No Intermediate Anode
Long. Velocity Spread	$\Delta v_z/v_z$ = $\pm$ 8%	$\pm$ 2.5 % Goal

As shown in Table II, the velocity spread goal for the new gun design was $\pm$ 2.5 percent standard deviation. To accomplish this, the cathode of the new gun was tilted to 40° to obtain a laminar flow beam, a single anode was used to provide direct acceleration to full beam potential, and a narrower strip cathode was utilized. All of these changes lead to diminished velocity spread related to electron ray optics and space-charge effects. The negative aspect of the design changes is the increased cathode current density which was not deemed excessive for an experimental device and therefore a worthwhile price to pay for a low velocity spread performance.

The design proceeded by utilizing the adiabatic MIG trade-off equations given in the previous Section II to determine the constants of design, and then the

values of the gun variables were determined by setting the cathode radius to 0.65 cm (same as the Seftor Gun). The position of the anode with respect to the cathode was adjusted to provide 70 kV (the full beam voltage) on the first (and only) anode. The results of the new electrode shapes with the Seftor gun electrode shapes superimposed, are shown in Figure 2.

The final electrode shapes shown in Fig 2 were determined by repeated computer simulations of the electron trajectories (using the Hermannsfeldt Code*) while successively making small changes in the anode and cathode shapes. More than 50 computer simulation runs were required for this procedure before a final design was achieved. The final electrode adjustments were made to the radius of curvature on the cathode which had the effect of changing the value of $v_{\perp c} = E_c \sin\theta_{EB}/B_c$ across the length of the cathode. Plots of ($\alpha = v_\perp / v_z$) versus ray number in the final compressed beam were used as the primary analysis tool for determining the effects of changes.

The final results of this cut-and-try optimization procedure are shown in Figures 3 and 4 which show an 8-ray beam simulation of the new gun and its α plot. The final velocity spread in the longitudinal direction taken from Figure III-3 is less than $\pm$ 0.5%. This is the electron ray optics contribution to the total velocity spread and it includes the space-charge effects of a 9 ampere beam current. When the beam current is reduced to smaller values, very little change in the velocity spread occurs.

In Figure 4, we have included the results from two non-optimized gun simulations to illustrate the optimization process. One shows the results

---

* Hermannsfelt (1973)

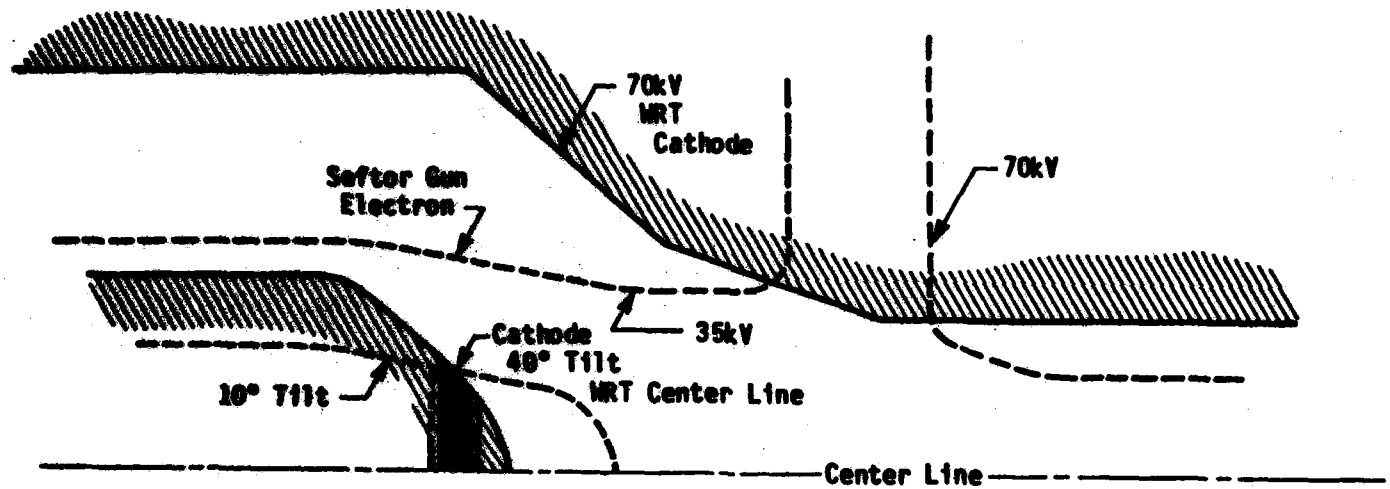

Figure 2. Comparison of New Single Anode Gun Electrode Shapes (solid line) with the previous Seftor Gun Double Anode Shapes (dashed line)

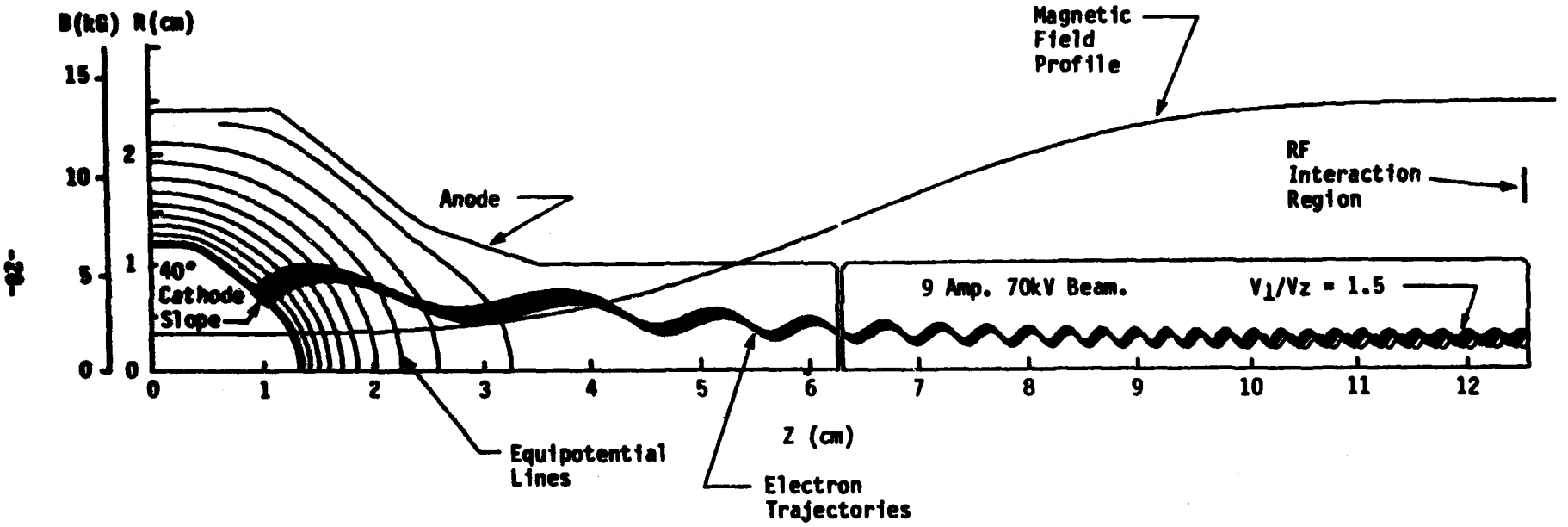

Figure 3. Single Anode Magnetron Injection Gun Design for NRL 35GHz TE_{01} GYRO-TWT

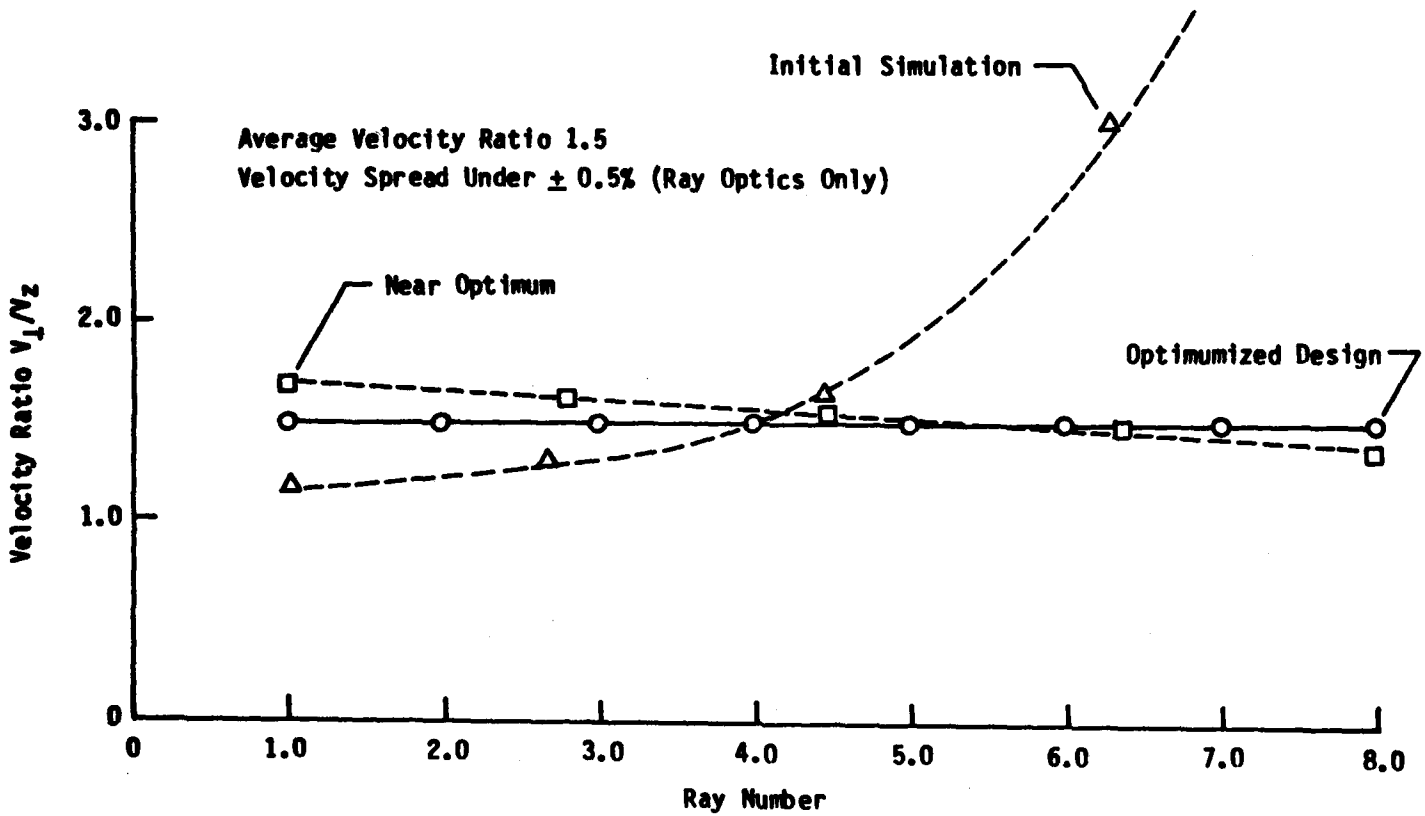

Figure 4. Final Velocity Ratios for the 8 Ray Simulation shown in Figure 3.

obtained on the first simulation using the adiabatic design values. One of the rays in this "first try" was reflected ($\alpha = \infty$), but the central ray was close to the desired design value. The other plot shows an intermediate result which was obtained prior to achieving the optimum design. Note that 5 electron rays were used during the optimization process and that the number of rays was increased to determine final beam performance.

Simulation of the temperature-limited gun was implemented by launching the electron rays normal to the cathode surface with each ray carrying a current proportional to the area on the cathode represented by the ray. Rays from the two edges carried approximately 1/2 current. This procedure gives an accurate simulation so long as there is a minimal depression of the electric field at the cathode due to space charge; i.e., so long as (I_0/I_L) is small.

Note in Figure 3 that a plot of the magnetic field is superimposed over the gun simulation. The cathode is placed in a flat magnetic field region designed into the superconducting solenoid at NRL. A trim coil in the solenoid permits the magnetic field in the cathode region to be adjusted experimentally.

Determination of the sensitivities of the gun to: (a) the axial position of the cathode with respect to the magnetic field and (b) to the adjustment of the field in the cathode region are of primary importance for experimental purposes. These sensitivities were obtained by computer simulation as shown in Figure 5. Note that the permitted variation in longitudinal position of the cathode is about 0.5 cm, over which distance reasonably low velocity spreads and the proper velocity ratio are maintained. The vertical bars in the plots show the extent of the spread for the simulation run, and the dots and the numerical percentages give the average velocity ratio and the longitudinal velocity spread respectively.

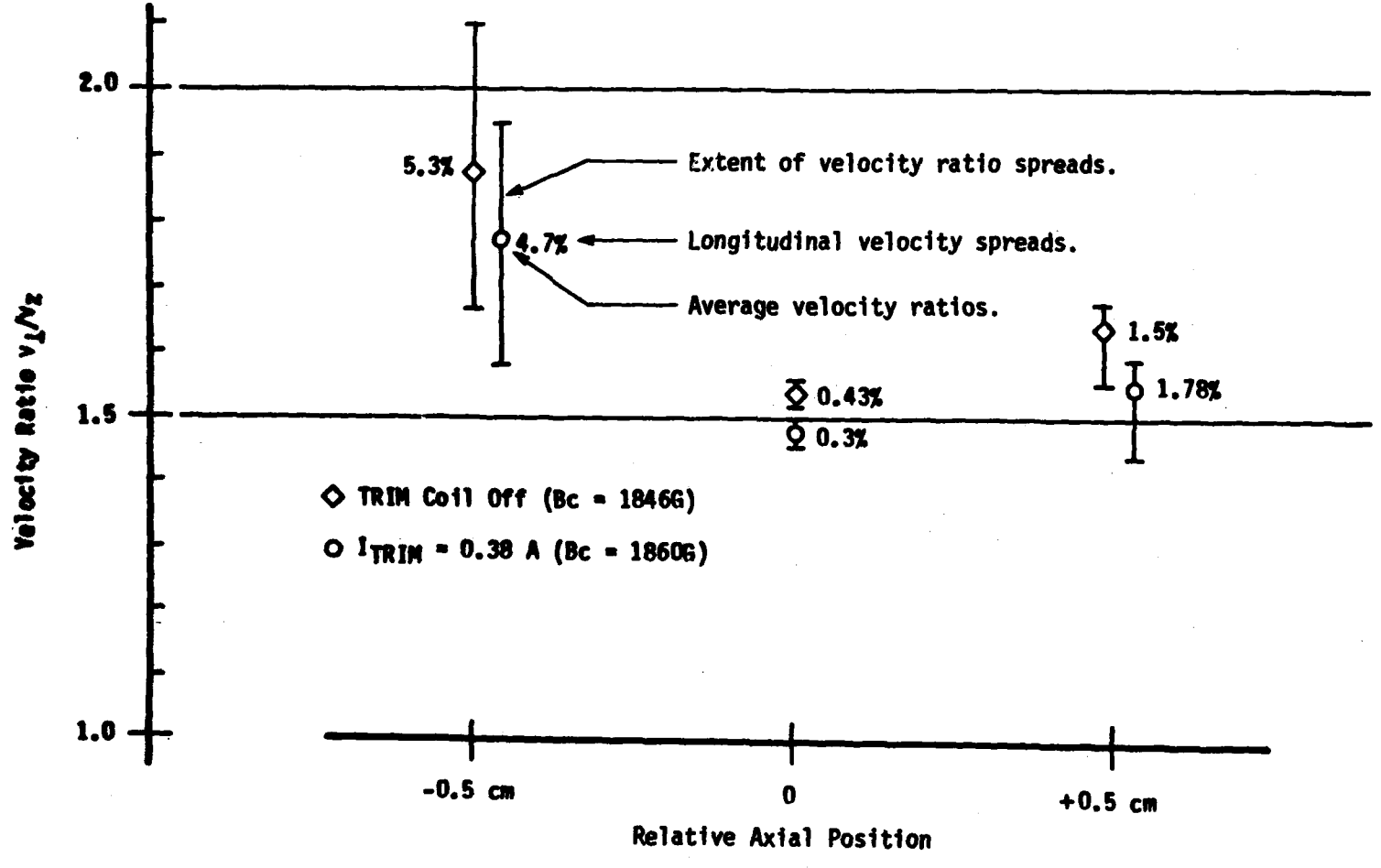

Figure 5. Sensitivity of Velocity Ratio and Spread to Longitudinal Position and Cathode Magnetic Field.

The data in Figure 5 can be re-plotted as a function of the cathode magnetic field to reveal more clearly the sensitivity of velocity ratio to this experimental parameter. The result is shown in Figure 6.

When $d\alpha/dB_z$ is calculated from adiabatic beam flow, the slopes of the theoretical sensitivity lines shown in Figure 6 are obtained. The simulation results show a good fit to adiabatic theory.

The final experimental parameter sensitivity which needs to be determined is that of beam voltage. Figure 7 gives the results of a plot of versus voltage. An adiabatic, non-relativistic theoretical sensitivity is shown in this figure also. The theoretical result fits the data reasonably well. Note that voltage and magnetic field adjustments can make substantial changes in without introducing excessive velocity spread.

EFFECTS OF CATHODE TEMPERATURE AND SURFACE ROUGHNESS

As the foregoing computer simulations show, the velocity spread due to electron ray optics (path differences) has been virtually eliminated in this gun design. Assuming that the simulation is correct*, the major contributions to velocity spread will come from the cathode temperature, Tc, and cathode surface roughness, R. The variable R in this case is the radius of a hemispherical bump on the cathode surface which is used to model the roughness. (See Appendix C.) In practice, it seems probable that using the characteristic surface roughness (or RMS roughness) for R will provide a reasonable estimate of the resulting velocity spread.

---

* Temperature-limited MIG simulations in the U.S.A. have not yet been experimentally verified by direct measurement on electron beams.

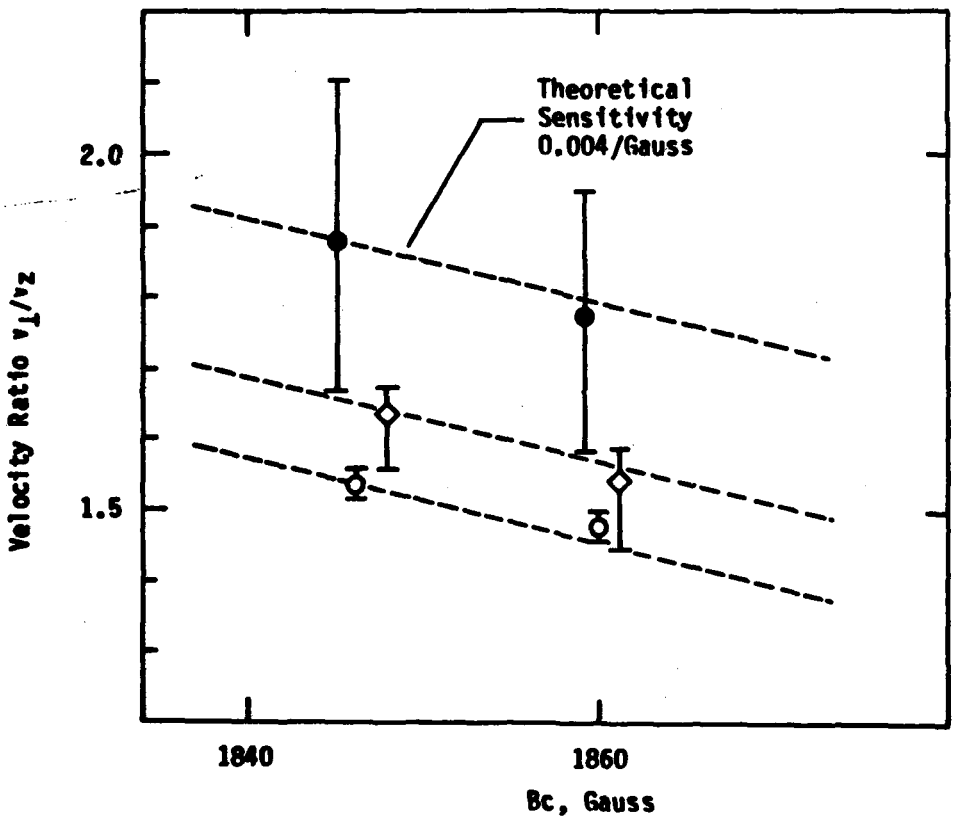

Figure 6. A Replot of Data in Figure 5 versus Cathode Magnetic Field.

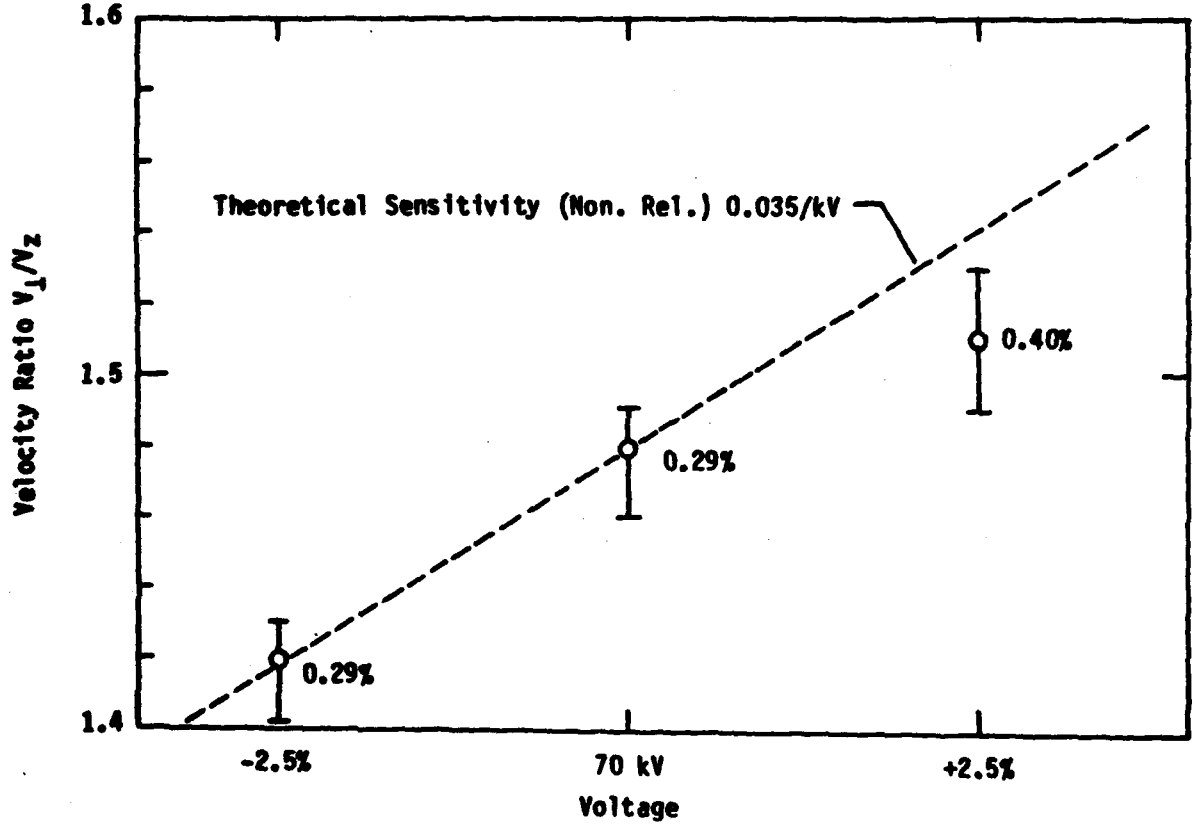

Figure 7. Plot of Velocity Ratio Sensitivity to Beam Voltage.

THIS PAGE INTENTIONALLY LEFT BLANK

The equations which provide estimates of velocity spread taken from Section II are

$$\left(\frac{\Delta v_\perp}{v_\perp}\right)_T r_c^{-1} = \pm \left[\frac{C_B(kT_c/m_o)^{\frac{1}{2}}}{C_E \cos(\phi_c + \theta_B)}\right] \equiv \pm C_T$$

$$\left(\frac{\Delta v_\perp}{v_\perp}\right)_R r_c^{1/2} = \pm \left[\frac{0.4\, C_B\sqrt{2nR}}{C_E^{1/2}\cos(\phi_c+\theta_B)}\right] \equiv \pm C_R$$

where the definition of the variables are given in Table Ib. For the gun design shown with T_c= 1200°K and R = 0.5 μm, these expressions can be evaluated to give

$$(\Delta v_z/v_z)_{T_c} = \pm\ 0.64\% \quad ; \quad (\Delta v_z/v_z)_R = \pm\ 2.5\%$$

When these two components of velocity spread are combined with the 0.5% spread due to ray optics, the RMS average velocity spread is $\pm$ 2.6%. This is the predicted total velocity spread assuming that a cathode roughness of 0.5 μm can actually be attained.

For a dispenser-type cathode, the surface roughness for commercial grade Type-B cathodes is on the order of 0.8 μm. We therefore anticipate that some special cathodes will have to be made to attain the desired $\pm$ 2.5% spread performance. For the commercial grade cathodes with the best possible polish, we anticipate an overall velocity spread closer to $\pm$ 3%. This is still a significant improvement over the previous available gun which had greater than $\pm$ 8% spread.

SECTION IV

STEPPED MAGNETIC FIELD FOR GYROTRON BEAM GENERATION

IV. STEPPED MAGNETIC FIELD FOR GYROTRON BEAM GENERATION

In this section, we first review the results of beam simulations using magnetic reversal and then give the results of some new work which shows that one of the oldest techniques used in gyrotron guns -- the variable transverse magnetic field kicker -- may have excellent properties for beam control which have not been previously illuminated and should be researched more thoroughly.

4.1 REVIEW OF FIELD REVERSAL

The interim report* on this program gave the details of a study exploring the use of field reversal as a means for implementing gyrotron guns. In that report it was concluded that the fundamental velocity spreading mechanism in the absence of space-charge arises from the spread in the initial radii of the electrons as they are emitted from the cathode. We repeat here the following three figures: Figure 8, the concept of field reversal used to generate a beam spiraling around the axis; Figure 9 the typical output of computer simulations of this mechanism, and Figure 10, a summary of final velocity ratio α versus initial radius for several cases simulated.

The results show that the fundamental velocity spreading mechanism is strong when large α is required. The first order theory for this spread is given by

$$\Delta v_z/v_z = \alpha^2 \, \Delta r_c/r_c \qquad (9)$$

which shows that the longitudinal velocity spread resulting from an ideal (infinitely sharp) field reversal is equal to the spread in the initial radii of the electrons emitted from the cathode multiplied by the square of

* Baird and Attard, 1980

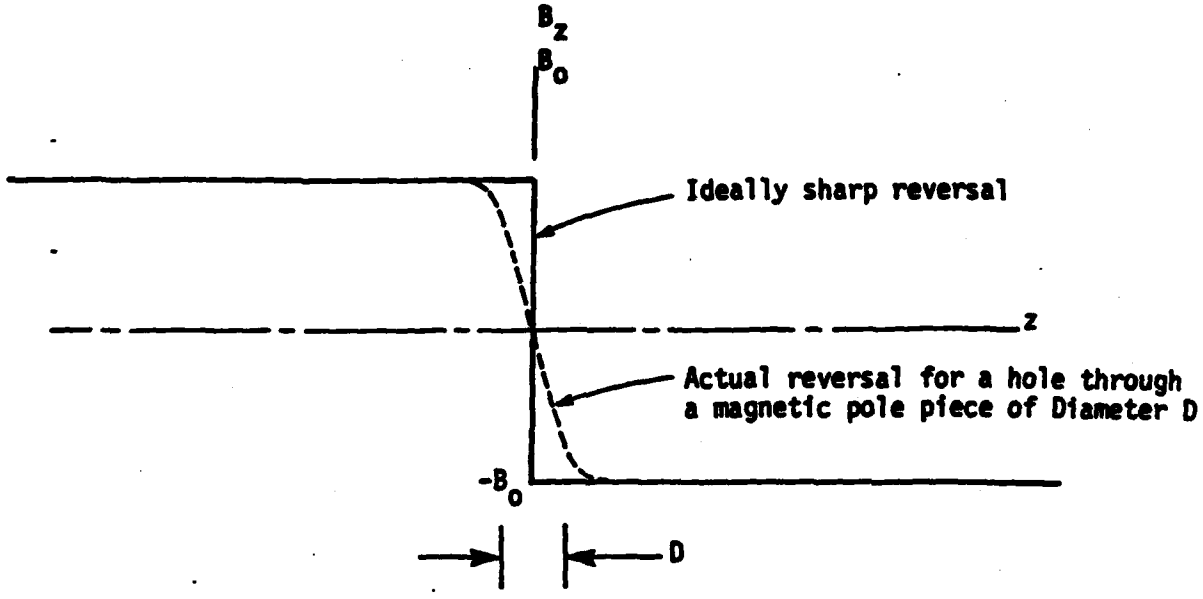

a) Magnetic Field Reversal

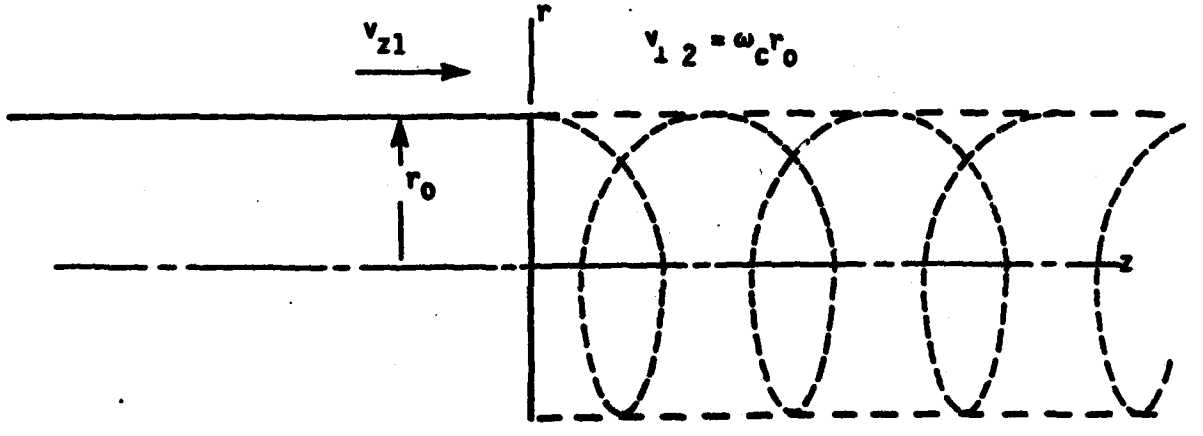

b) Electron Trajectory Through Ideal Field Reversal.

Figure 8. Generation of a Rotating Beam via a Field Reversal (Magnetic Cusp in Radial Field)

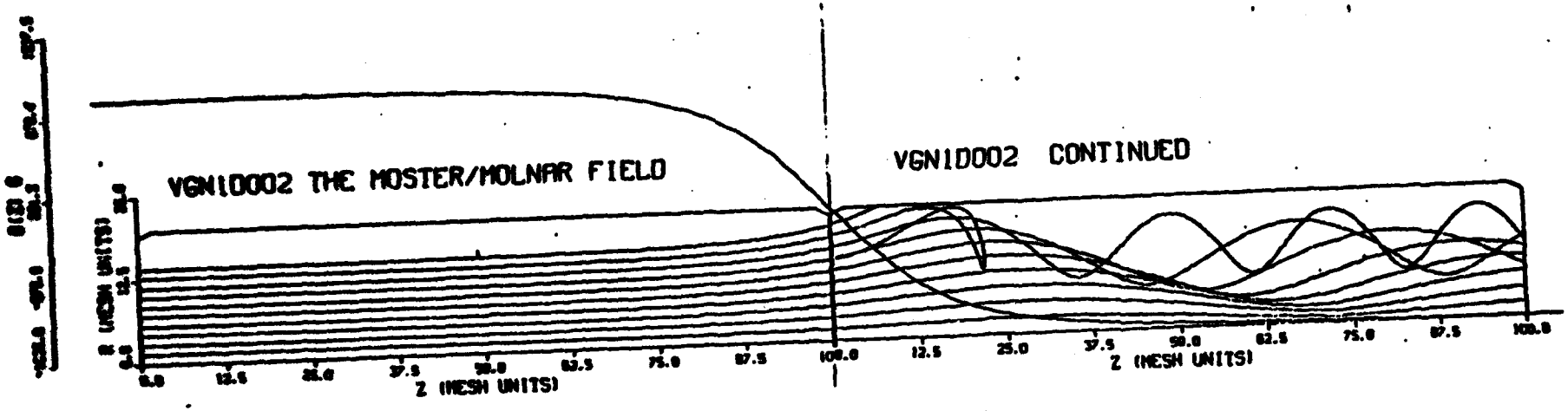

(a) General characteristics of electron rays passing through the field reversal.

(b) Annular beam having annulus equal to 10% of beam radius.

α(max)=2.2, α(min)=1.5, α(ave) = 1.82

Total $\Delta v_z/v_z$ = 29%, Standard Deviation = 9.1%

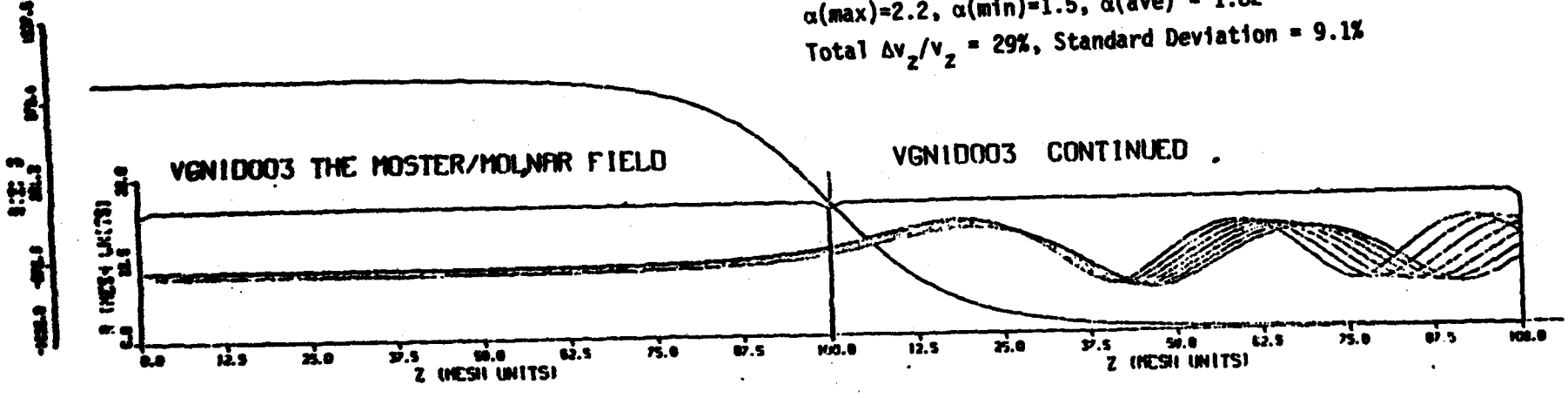

Figure 9. Computer Simulation of Magnetic Field Reversal for Generation of Electron Beams for Gyrotrons

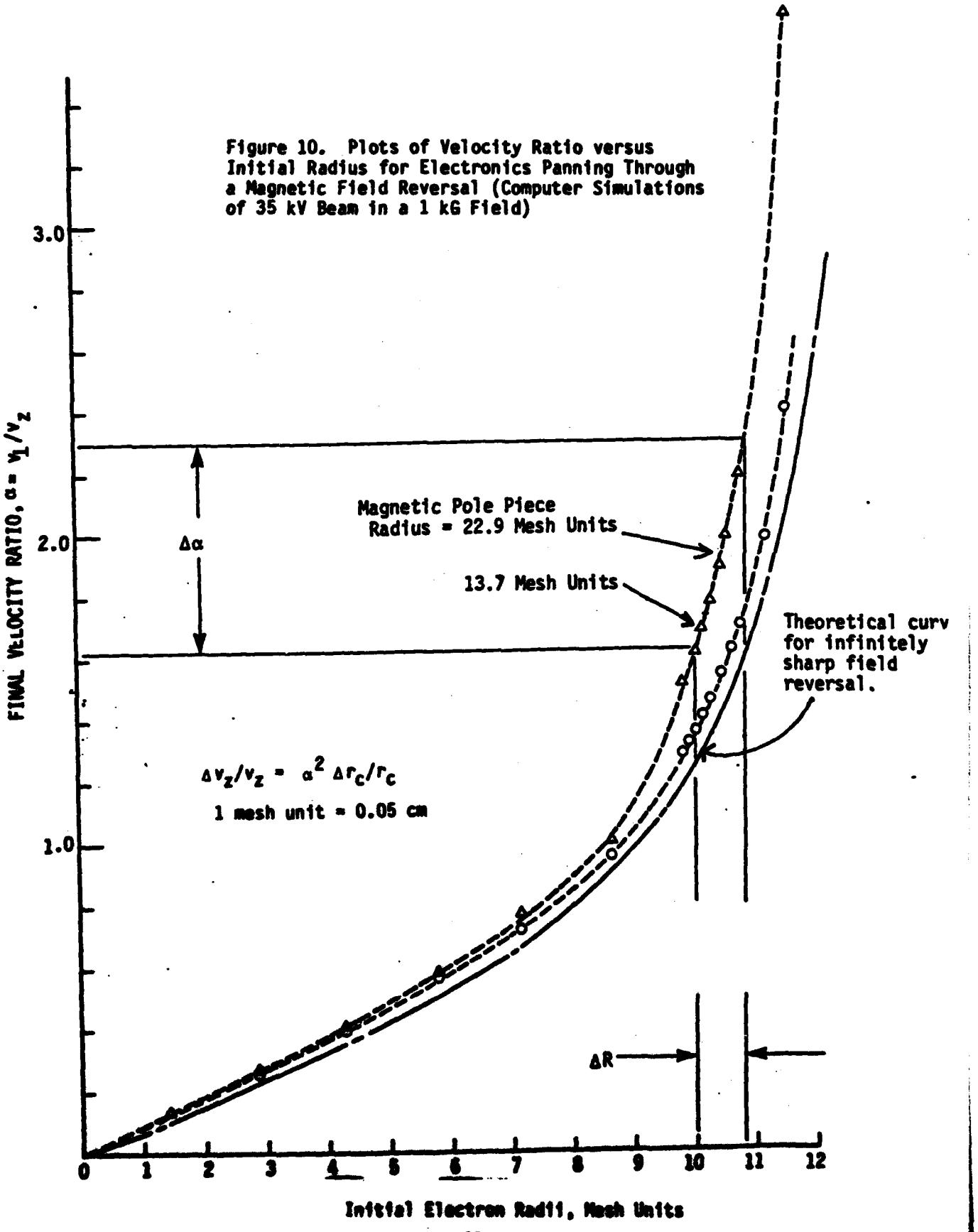

Figure 10. Plots of Velocity Ratio versus Initial Radius for Electronics Panning Through a Magnetic Field Reversal (Computer Simulations of 35 kV Beam in a 1 kG Field)

α. Thus if $\alpha = 2$, $\Delta v_z/v_z = 4\Delta r_c/r_c$ which makes it very difficult to get spreads on the order of a few percent. Figure 10 shows that in realistic cases of finite length field reversal, the spread gets slightly worse.

Schemes in which one begins with a small magnetic field and a large annular cathode ring and subsequently compresses the beam do not alter the first order theory for spread -- one simply uses the final α of the compressed beam in the calculation. Such schemes greatly improve the possibilities for attaining low velocity spread because $\Delta r_c/r_c$ can be made smaller; but, it still looks difficult to reach values of $(\Delta v_z/v_z)$ on the order of 1 or 2% as desired for amplifier applications.

We previously concluded in the interim study report that although field reversal beam generation may have applications in gyromonotron oscillators, it looked doubtful for amplifier applications because of the ultra-low velocity spreads required in these long devices. Since the time of our interim report, it has been suggested that the inclusion of significant amounts of space-charge in the beam may alter the above results significantly in a manner which will change the velocity spreading mechanism in favorable ways. No additional computer simulations have been carried out during this study program to either confirm or refute this idea. This idea should be explored in any future studies of the field reversal mechanism for gyrotron applications.

It is noted that a new study by Scheitrum (1981) shows that shaping of the field reversal by adding perturbing pole-pieces on either side of the field reversing pole can significantly alter and virtually eliminate the ripple on the generated spiraling beam. No investigation was made of the resulting effects on the basic velocity spreading mechanism, but this also should be explored in any future work.

4.2 THE VARIABLE TRANSVERSE MAGNETIC FIELD KICKER FOR GYROTRON BEAM GENERATION AND CONTROL

There is still a strong need in gyro-TWT applications for a small spiraling beam with low velocity spread. One example where such a beam is desirable is the fundamental mode TE_{11} gyrotron in which the waveguide circuit is considerably smaller than any circular mode gyrotron and in which the electric vector extends across the waveguide. This type of gyrotron will be useful in radar amplifier applications because: (1) its gain per unit length is the highest of all possible modes, (2) velocity spread will be less damaging because the tube will be shorter for a fixed value of gain, (3) wide band coupling into the fundamental mode circuit is simplified, and (4) a circularly polarized wave can be amplified.

Because magnetic field reversal appears to be prone to large velocity spreads, other techniques to achieve low velocity spread are being explored. We report here a more detailed study of one of the early guns utilized by Chow and Pantell (1960) for cyclotron device research. The analysis technique utilized is again the stepped magnetic field approach which produced surprisingly accurate results in the field reversal analysis. The results on the Chow and Pantell gun show that velocity spread can most likely be reduced to the range of a few percent and this appears to have been verified by Chow and Pantell. Their report indicated that full beam transmission was achieved at $\alpha = 8$. This would require a velocity spread on the order of 1%.

The basic configuration of the gun is illustrated in Figure 11. The ring cathode is shielded from the magnetic field by a magnetic envelope which

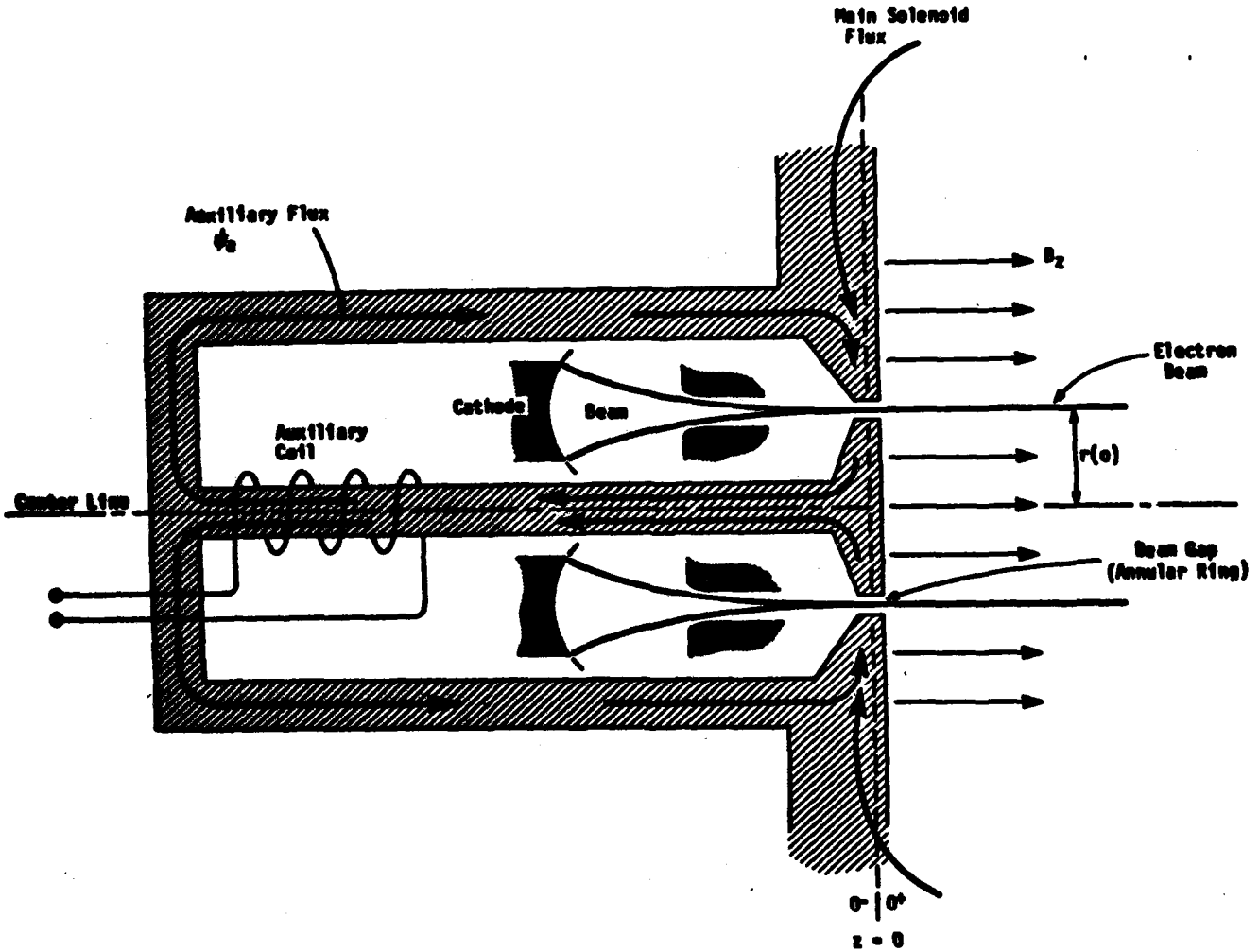

Figure 11. Conceptual Drawing of a Variable Transverse Magnetic Kicker Gyrotron Gun (see Chow & Pantell, 1960)

has a magnetic pole piece running up through the center of the cathode. The electrons are focused electrostatically into a thin annular beam which exits from a circular slit in the face of the magnetic pole piece extending perpendicular to the beam axis. This latter pole piece carries magnetic flux from two solenoids: (1) from the main solenoid to the right of the gun which produces a uniform magnetic field emanating to the right of the pole face, and (2) from an auxiliary flux coil which is inside the gun shield and produces a variable transverse flux across the gap where the beam enters the magnetic field. This auxiliary flux is the key to launching a beam which rotates uniformly about the axis of the device. As will be seen, it also provides control of the α in the beam.

4.2.1 Beam Geometry Analysis

We begin the analysis by looking at the transverse and longitudinal fields in the pole piece gap where the beam exists from the gun. To use the stepped magnetic field approach, we make the approximation that the width of the output pole piece is negligible so that all of the radial flux in the gap occurs at the single position z = 0. This corresponds to a stepped function in the magnetic potential at z = 0 and we utilize the Heaviside unit step function u(z) for this purpose*.

$$u(z) = \begin{matrix} 0 \\ 1/2 \\ 1 \end{matrix} \begin{cases} \text{for } z < 0 \\ \text{for } z = 0 \\ \text{for } z > 0 \end{cases} \qquad (10)$$

* M. Abramowitz and I. A. Stegun, Handbook of Mathematical Functions, U.S. Government Printing Office, 1964, p. 1020.

In terms of this function the magnetic potential which supports both the main magnetic field and the added flux in the gap produced by the auxiliary coil is given by

$$A_\theta = rB_z u(z)/2 + \psi_a u(z)/2\pi r \tag{11}$$

Here, the first term applies to the main field which exists only for $z > 0$ and the second term applies to the auxiliary field which, insofar as the beam is concerned only exists as a transverse flux ψ_a at the position $z = 0$. To see that Equation 11 gives the correct results one simply applies $\vec{B} = \nabla X \vec{A}$ to obtain the magnetic flux density and $\psi = \int_s \vec{B} \cdot \vec{ds}$ to get the magnetic flux passing through a pole surface s.

Using the relationships

$$du/dz = \delta(z) = \text{Dirac delta function}^*$$

$$\int_{0^-}^{0^+} f(z)\,\delta(z)dz = f(0) \tag{12}$$

$$\int_{0^-}^{0^+} u(z)\,\delta(z)dz = u(0) = 1/2$$

one gets for the magnetic field

$$\vec{B} = -\left(rB_z\delta/2 + \psi_a\delta/2\pi r\right)\hat{r} + (B_z u)\hat{z}, \tag{13}$$

where $\hat{r}$ and $\hat{z}$ are unit vectors, and for the transverse magnetic flux in the gap

$$\psi(\text{gap}) = -\pi r_g^2 B_z - \psi_a \tag{14}$$

The first flux term on the R.H.S. of equation 14 is the radial flux which supports the main field inside the gap radius r_g. The second term is

---

* J. D. Jackson, Classical Electrodynamics, John Wiley & Sons, Inc., New York, 1962, pp. 3-4.

simply flux from the auxiliary coil. Note that both fluxes have the same sign so that a positive ψ_a is in a direction which aids the gap flux due to the main solenoid.

We now use conservation of angular momentum to determine the effects of the magnetic field on the beam. Putting A_θ from equation 11 into

$$[r^2\dot{\theta} - (e/m_0)rA_\theta] = 0 \qquad (15)$$

(which assumes that both $\dot{\theta}$ and A_θ are zero at $z = 0^-$,) we can rearrange terms and evaluate the expression for $z > 0$ to get

$$e\psi_a/2\pi m_0 = \gamma r^2\dot{\theta} - eB_z r^2/2m_0 \qquad (16)$$

Then, the R.H.S. of Equation 16 can be re-written in terms of the beam geometry parameters (see Appendix B) to get

$$\psi_a/\pi = B_z\,(a_+^2 - b_+^2) \qquad (17)$$

Where a_+ is the cyclotron radius and b_+ is the guiding center of the electrons evaluated at the position $z = 0^+ > 0$.

Note from Equation 17 that if $\psi_a = 0$ then $a_+ = b_+$ and the electrons rotate through $r = 0$ (i.e., the z axis). This is very undesirable because the resulting high space charge would produce severe velocity spreading effects. Note also, that if ψ_a is positive, then $a_+ > b_+$ and the beam circles the z axis. If ψ_a is negative, $b_+ > a_+$ and an annular beam such as that produced by NIBs is achieved.

To determine the relative sizes of a_+ and b_+, we go to the z equation of motion obtained from the Lagrangian for relativistic electron motion in cyclindrical static fields. (See Appendix B.)

$$\ddot{z} + (e/m_0\gamma)\, r\dot{\theta}\, \partial A_\theta/\partial z = 0 \qquad (18)$$

Using Equations 11 and 15 this becomes

$$\ddot{z} = -(e/\gamma m_0)^2 [rB_z/2 + \psi_a/(2\pi r)]^2\, u(z)\, \delta(z)$$

which upon substitution of $\ddot{z} = (1/2)d(\dot{z})^2/dz$ can be integrated through the gap from $z = 0^-$ to $z = 0^+$ to get

$$v_{z+}^2 - v_{z-}^2 = -1/4\, (e/m_0)^2 \left[r(o)B_z + \psi_a/\pi r(o)\right]^2 \qquad (19)$$

where r(o) is the electron radius at the position z = 0. Equation 19 gives the change in the z velocity as the beam enters the magnetic field through the gap. Note that the velocity change depends on two field factors B_z and ψ_a with ψ_a being experimentally variable.

To proceed with the analysis, we now re-write equation 19 in the form

$$v_{z-}^2 - v_{z+}^2 = v_\theta^2 \qquad (20)$$

where

$$v_\theta^2 = (1/4)\omega_c^2 r^2(o)(1+F_R)^2 \qquad (21)$$

and F_R is the magnetic flux ratio in the gap

$$F_R = \phi_g/(\pi r^2(o)B_z) \tag{22}$$

Rewriting Equation 20 in terms of perpendicular velocities gives

$$v_{\perp_+}^2 = v_{\perp_-}^2 + v_\delta^2 \quad . \tag{23}$$

This is the desired relationship giving the increase in transverse velocity as a result of the beam passing through the gap.

It must be recognized in Equation (23) that the maximum value for perpendicular velocity is $v_{\perp_+}=v_o$. If one tries to make $v_{\perp+}$ too large, reflection will occur. It should also be noted that $v_{\perp-}$ can only be a velocity component in the radial direction since the analysis has proceeded on the assumption that $\dot{\theta}(z = 0^-)= 0$. It is therefore permissible in the analysis for the beam to enter the gap at a converging angle with respect to the axis so long as no θ motion is involved.

For a quasi-longitudinally directed beam in which $v_\delta^2 >> v_{\perp-}^2$, we can neglect $v_{\perp-}$ and immediately determine the geometry of the output beam from Equations 21 and 23.

$$a_+ = v_{\perp+}/\omega_c = (r(o)/2)\ (1 + F_R) \tag{24}$$

Then from Equation 17 and after some algebra

$$b_+ = (r(o)/2)(1 - F_R) \tag{25}$$

These equations can be inverted for design purposes to give

$$F_R = (a_+ - b_+)/(a_+ + b_+) \qquad (26)$$

$$r(o) = a_+ + b_+ \quad . \qquad (27)$$

From these two equations it is evident that the conditions which give a beam circling the axis (i.e., $b_+ = 0$) are $F_R = 1$ and $r(o) = a_+$. Thus, the auxiliary flux must equal the main solenoid flux in the gap (i.e., double the radial field) and the beam radius in the gap must equal the desired Larmour radius in the main field at the position $z = 0^+$.

Once a gun of this type is fabricated, it is interesting to contemplate the effect of changing the auxiliary flux during operation. Since r(o) is fixed, Equations 24 and 25 show that a_+ and b_+ change directly with F_R. Since the transverse velocity $v_{\perp +} = \omega_c a_+$, the result is a direct change in beam α. The sensitivity to this change has been calculated to be

$$\Delta\alpha/\alpha = (\alpha^2 + 1)\,[F_R/(1 + F_R)]\,\Delta F_R/F_R \qquad (28)$$

At $\alpha = 1.5$ and $F_R = 1$, this equation says that a 10% change in auxiliary flux will produce a 16% change in α. The change in v_{z+} would be 11%. This type control could be a significant factor in improving the flexibility of experimental optimization of gyrotron devices.

An even more surprising fact is that the overall beam size which is given by $(a_+ + b_+)$ is independent of F_R. This says that while α is changing the overall beam size remains the same.

2. Velocity Spread Analysis

If we differentiate Equation 23 to determine the sensitivity of the perpendicular velocity spread to the gun parameters in the gap region, we get (assuming again $v_z^2 \gg v_{\perp -}^2$)

$$\Delta v_{\perp +}/v_{\perp +} \approx (v_{\perp -}/v_z)^2 \ (\Delta v_{\perp -}/v_{\perp -}) + \Delta v_z/v_z \qquad (29)$$

Equation 29 immediately reveals that the velocity spread ($\Delta v_{\perp -}/v_{\perp -}$) associated with the beam converging into the magnetic gap has negligible effect on the output velocity spread because of the multiplying factor of $(v_{\perp -}/v_z)^2$. Thus, the main contribution will most likely come from $\Delta v_z/v_z$.

Differentiating Equation 21 with respect to r(o) we get

$$\Delta v_z/v_z = \Delta r(o)/r(o) \qquad (30)$$

So that finally

$$\Delta v_{\perp +}/v_{\perp +} \approx \Delta r(o)/r(o) \qquad (31)$$

This is identical with the velocity spread equation for the field reversal case with one notable exception. The radius "r(o)" in equation 31 is the radius of the beam in the gap whereas previously it was the radius at the emitting cathode. Since the present scheme can take advantage of electrostatic focusing to make $[\Delta r(o)/r(o)]$ very small, it appears that low values of velocity spread should be achievable.

The sources of velocity spread which have been neglected in this analysis are those due to fringing fields, a finite gap length, cathode temperature, and

space change. These will most easily be determined by computer simulations which have not been carried out for this gun during this study program. Because the fundamental velocity spreading mechanisms appears to be favorable, however, there is reason to be optimistic that low velocity spreads could be achieved.

4.2.3 Alternate Gun Geometry

Equation 23 shows that it is possible to achieve the desired transverse velocity $v_{\perp +}$ by using $v_{\perp -}$ alone. This would require that $v_\delta = 0$ (i.e., $F_R = -1.$). In this case the auxiliary coil is used to reduce the flux in the gap to zero so that the transverse velocity of the beam passing through the gap is unchanged. Such a beam would be designed to pass through the gap with a convergence angle sufficiently large to give the desired $v_{\perp +}$.

One important advantage of this concept is the extra room that it gives in the cathode area to provide a high voltage standoff between the cathode and the central magnetic pole piece. Voltage breakdown in this area was the failure mode of the original Chow and Pantell gun.

One of the disadvantages is the fact that the output velocity spread is no longer insensitive to the spread in convergence angle of the electrons entering the gap. In fact,

$$\Delta v_{\perp +}/v_{\perp +} \simeq (\Delta v_{\perp -}/v_{\perp -}) - (\phi_e/\tan\phi_e)\Delta\phi_e/\phi_e \qquad (32)$$

Where ϕ_e is the axial angle of the electrons entering the gap. This could be a severe drawback in some design cases.

Overall, it appears that there could be a design regime in which the best of both schemes could be used. A convergent beam in the gap may be possible while still maintaining $v_z^2 \gg v_{\perp -}^2$.

In any case, it appears to be important to use a converging electron beam in the gun in order to get high voltage standoff. The velocity spread may deteriorate somewhat, but the ability to experimentally change α using the auxiliary coil would still be retained in any such design.

It should be understood that the beam design parameters in the gun region of the foregoing discussion ($z = 0^+$) may or may not be the desired rf interaction values. For millimeter wave tubes where large magnetic fields are needed, one would be required to utilize an adiabatic beam compression region to transform the beam parameters at the output of the gun into those desired for rf interaction.

SECTION V

CONCLUSIONS AND RECOMMENDATIONS

V. CONCLUSIONS AND RECOMMENDATIONS

Conclusions

We conclude this final report on the gyrotron gun study program by providing the following summary of accomplishments:

1. A complete review and analysis of the magnetron injection gun (MIG) type gyrotron was carried out including a review of the extensive Soviet literature.

2. Design trade-off equations were developed which provide initial design points for MIG computer simulations. These equations, which are based on adiabatic beam flow, have been extended to include arbitrary cathode tilt angle. Without these initial design calculations, computer simulations become very difficult to implement because of the complexity of the beam flow.

3. The design was completed for a single-anode MIG-type gyrotron gun to be used in the NRL 35 GHz gyro-TWT experiments. Computer simulations of this gun indicate that it will have significantly reduced velocity spead. This gun is now in the final stages of assembly and will be used as a direct replacement for the existing NRL gun to improve efficiency in the gyro-TWT. The anticipated velocity spread is $\pm$ 2.5% which is a factor of 3 to 5 less than the existing gun.

4. A stepped magnetic field theory has been utilized for analysis of the fundamental velocity spreading mechanisms in transverse magnetic field "kicker" approaches to gyrotron beam formation. Using this technique we have identified the basic spreading mechanisms for the field reversal and the shielded cathode schemes. In both cases, this spreading mechanism is proportional to the spread in the radial position of the electrons at key points along the beam. It was shown that the shielded cathode approach holds promise for applications requiring low velocity spread because it permits electrostatic beam focusing which can significantly reduce the radial spread at the key point of magnetic field entry.

   In addition, a shielded gun with an auxiliary field coil has been shown to provide very attractive properties for experimental control of the beam. In this case, the velocity ratio can be varied over a wide range while the beam size remains constant.

The details of these accomplishments are contained in Section II through IV of this report with additional backup material in the three appendices provided. We have endeavored to make this a self contained report by incorporating pertinent data and materials from the interim report (Baird and Attard, 1980).

Recommendations

A number of interesting avenues for further research in the general area of gyrotron beam formation are evident as a result of this study program. Four of these are enumerated as follows:

1. The fact that gun simulation codes are mandatory in the analysis and optimization of gyrotron guns raises the many questions about the utility of these codes and accuracy of the simulations achieved. We recommend that a coordinated program to develop interactive, graphics-oriented codes in conjunction with a demountable beam test facility be started immediately. These tools would permit a coordinated effort between gun simulations and physical measurements which would be extremely beneficial in the R&D effort to produce high performance and high power gyrotron guns. The demountable beam test facility should provide for scaling the test guns in both voltage and size so that the performance of high power beams and physically small beams can be measured.

2. Additional computer simulation work should be carried out on the NRL single anode MIG design to evaluate two properties of the gun which need to be further investigated. First, it would be very valuable to determine the thermal velocity spread in the gun by direct simulation. This can be accomplished be adding additional electron rays to the simulation which have initial transverse energies equal to the mean thermal velocity. Such a simulation would help provide verification

of the expected velocity spread performance of this gun which is predicted to be almost totally due to initial transverse velocities at the cathode (due to thermal effects and cathode roughness).

The second design feature of the NRL MIG which needs to be investigated through computer simulation is the effects of a modulation anode placed along an equipotential line near the cathode. Such an anode would be extremely useful in systems applications to provide beam current modulation. It should be possible to determine the major effects of such an anode on the beam performance through computer simulation.

3. The properties of the shielded cathode gun with a transverse magnetic field "kicker" described in Section IV B needs further investigation. The first order analysis given in this report shows excellent promise that this type gun can provide both exceptional beam control and low velocity spread. It is recommended that designs which employ a slightly converging electron beam (decreasing beam radius at the magnetic pole piece) be investigated because this configuration will produce the lowest possible velocity spread while still giving some relief to the high voltage standoff portion problem inherent in this type gun. A computer simulation should be utilized which can give a good simulation of the fringing magnetic fields at beam exit point (lens effects) as well as simulate thermal velocities in the beam.

4. The Soviet literature survey given in Appendix A demonstrates the importance of the high power MIG synthesis approach utilized by Tsimring (1977) and Manuelov and Tsimring (1979). In this approach, varying amounts of space-charge up to the space-charge limit are included in the analysis of an oscillating laminar flow beam which is accelerated away from the cathode. The gun electrodes which support this flow are then synthesized as equipotential surfaces outside of the beam. It is recommended that the computer codes required to perform this high power MIG synthesis be written and that they be utilized in conjunction with MIG computer simulations to investigate the high power limits of these type guns.

BIBLIOGRAPHY

BIBLIOGRAPHY

Avdoshin, E. G., L. V. Nikolaev, I. N. Platonov, and Sh. E. Tsimring, "Experimental Investigation of the Velocity Spread in Helical Electron Beams," Radio-Physics and Quantum Electronics, vol. 16, pp. 461-466, 1973.

Baird, J. M. and K. Amboss, "90 GHz Power Tube Technology Study," Hughes Research Laboratory, Malibu, California. Contract F33615-77-C-1240. Final Report, July 1978.

Baird, J. M., and A. C. Attard, "Design of a Single-Anode, MIG-Type Gyrotron Gun for a 35 GHz Gyro-TWT," 1981 IEEE Microwave Theory and Techniques Conference, Los Angeles, CA June 15-17 1981.

Baird, J.M., and A. C. Attard, "Gyrotron Gun Study Program -- Interim Report, B-K Dynamics, Inc., Rockville, MD, Prepared for the National Research Laboratory, Contract No. N00173-79-C-0132, July 1980.

Barnett, L. R., et. al., "Gain, Saturation, and Bandwidth Measurements of the NRL Traveling Wave Amplifier," IEDM Technical Digest, Washington, D.C., December 3-5, 1979, pp 164-167.

Barnett, L. R., et. al., "A High Gain Single Stage Gyrotron Traveling Wave Amplifier," IEDM Technical Digest, Washington, D.C., Dec. 8-10, 1980, pp. 314-347.

Barnett, L. R., et. al., "An Experimental Wide-Band Gyrotron Traveling-Wave Amplifier", IEEE Transactions, Vol. ED-28, pp. 872-875, July 1981.

Chow, K. K. and R. H. Pantell, "The Cyclotron Resonance Backward-Wave Oscillator," Proc. IEEE, Vol. 48, pp. 1865-1867, November, 1980.

Dickson, W, L. and C. C. Johnson, A Ten Kilomegacycle Amplifier Utilizing the Interaction Between a Periodic Electron Beam and an Unloaded Waveguide Mode, Department of Electrical Engineering, University of Utah, Salt Lake City, Utah Technical Report ASD-2, September 1964.

Dryden, V. W., "Exact Solutions for Space-Charge Flow in Spherical Coordinates with Application to Magnetron Injection Guns," JAP, vol. 33, p. 3118, October 1962.

Gaponov, A. V., A. L. Gol'denberg, D. P. Grigor'ev, T. B. Pankratova, and M. I. Petelin, "Induced Synchrotron Radiation of Centimeter Band Gyrotrons," Radiophysics and Quantum Electronics, vol. 16, no. 1, pp. 106-111, January 1973.

Harker, K. J., "Determination of Electrode Shapes for Axially Symmetric Electron Guns," JAP, vol. 31, p. 2165, 1960.

Harker, K. J., "Electrode Design for Axially Symmetric Electron Guns," JAP vol. 33, p. 1861, 1962.

J. L. Hirshfield, I. B. Bernstein and J. M. Wachtel, "Cyclotron Resonance Interactions of Microwaves with Energetic Electrons," IEEE Journal, vol. QE-1, No. 6, pp. 237-245, September 1965.

Kino, G. S. and N. J. Taylor, "The Design and Performance of a Magnetron Injection Gun," IRE Trans., vol. ED-9, p. 1, 1962.

Korolev, F. A. and A. F. Kurin, Cyclotron-Resonance Maser with a Fabry-Perot Cavity, Radio Engineering and Electronic Physics, vol. 15, no. 10, pp. 1868-1873, 1970.

Langmuir, I and K. B. Blodgett, "Currents Limited by Space-Charge Between Coaxial Cyclinders", Physical Review Series 2, Vol. 22, pp. 347-356, 1923.

Manuilov, V. N. and Sh. E. Tsimring, "Synthesis of Axially Symmetrical Systems for Shaping Helical Electron Beams," Radio Engineering and Electronic Physics, vol. 24, p. 111, 1979.

Shivley, J., C. Connor, F. Friedlander, E. Galli, H. Jory, D. Stone, R. Symons and G. Wendell, "EBT-P 110 GHz Development Program," Varian Associates, Inc., Palo Alto, California, Contract No. W7405-eng 26 Quarterly Report No. 1, September 1979.

G. P. Scheitrum, "High Rotational Energy Hollow Beam Design Using a Triple Pole Piece Magnetic Field Reversal," Stanford University, Department of Electrical Engineering, Engineering Degree Thesis, May, 1981.

R. L. Schriever and C. C. Johnson, "A Rotating Beam Waveguide Oscillator," Proc. IEEE (Correspondence), Vol. 54, No. 12, pp. 2029-2030, December 1966.

J. L. Seftor, et. al. "The Electronic Cyclotron Maser as a High-Power Traveling Wave Amplifier of Millimeter Waves," IEEE Transactions, 1979.

J. L. Seftor, A. J. Drobot, and K. R. Chu, "An Investigation of a Magnetron Injection Gun Suitable for Use in Cyclotron Resonance Masers," IEEE Transactions, Vol. ED-26, pp. 1609-1616, October 1979.

Sh. E. Tsimring, "Synthesis of Systems for Generating Helical Electron Beams," Radiophysics and Quantum Electronics, Vol. 20, pp. 1550-1560, 1977.

R. C. Wigerson, "'Corkscrew', -- A Device for Changing the Magnetic Moment of Charged Particles in a Magnetic Field," Physical Review Letters, Vol. 6, No. 9, pp. 446-448, May 1, 1961.

APPENDIX A

CHRONOLOGICAL REVIEW OF SOVIET GYROTRON GUN DEVELOPMENT

APPENDIX A

CHRONOLOGICAL REVIEW OF SOVIET GYROTRON GUN DEVELOPMENT

This review was first published in essentially the same form in the Gyrotron Gun Study Program Interim Report (Baird and Attard, 1980). It is included here because the body of literature encompassed contains valuable insights into the theory, measurement, and synthesis of gyrotron beams resulting from the intensive R&D effort in the U.S.S.R. over the past fifteen years. The much newer U.S. R&D effort can greatly benefit from a thorough review of the Soviet work. A number of design considerations and techniques are revealed which go beyond any work yet done in the U.S. and which need to be explored further.

The first detailed Soviet gun design and measurement studies started to appear in print in 1972, although crude versions of the MIG (magnetron injection gun) were used in the mid 1960's. (Figure A-1(a) shows a conceptual drawing of an early gun used by Gaponov, et al., 1965.)

1. Electron Trajectory Analysis

Two companion papers by Lygin and Tsimring in 1972 give the first analysis of Soviet MIGs for gyrotron application. Figures from the first paper are reproduced in Figure A-1. Figure A-1(b) shows the basic configuration of the type of gun analyzed, which has a strip cathode on an inclined inner electrode and a single anode which forms a quasi-coaxial magnetron type gun region. Figures A-1(c) through (d) show two versions of this gun, each with two different angles on the cathode electrode with respect to the symmetry axis. The first version uses an anode whose profile has a sharp corner; the second uses a smoothly varying profile. The equipotential surfaces shown were calculated by assuming a rectangular geometry approximation and using analytic techniques.

The second paper, whose figures are reproduced in Figure A-2, uses the calculated electrostatic fields and the magnetic fields of an air core solenoid to determine the electron trajectories from various assumed cathode positions. In this paper, the velocity spread between pairs of trajectories representing emission from the two extreme edges of a cathode was compared both by adiabatic analysis and direct numerical integration. It was determined that large differences exist in the degree to which adiabatic theory holds (i.e., the adiabaticity of the field configurations) and that "systems with smooth electrode configurations permit significant reduction in the spread of oscillatory velocities." Arrangements such as those presented in Figure A-2(c) were shown to have a particularly large velocity spread.

It is stated in the second paper that tilting the cathode at a large angle has the beneficial effect of creating a laminar flow beam which is less sensitive to the velocity spreading effects due to space-charge, and that the strip cathode can be placed over a wide range of positions along the central electrode surface provided that the magnetic field at the cathode is adjusted accordingly. It is also stated that an additional increase in the beam potential at some point downstream may or may not be required depending on the specific application. It is assumed that if a second longitudinal acceleration gap (second anode) is used, it will produce additional unspecified beam spread depending on its position and voltage difference.

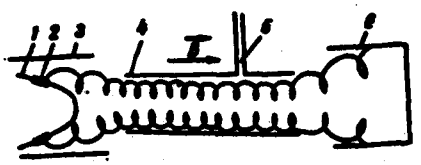

Helical beam CRM oscillator:
1) cathode, 2) emission zone,
3) anode, 4) cavity, 5) output
waveguide, 6) collector.

a) Experimental Gyrotron by Goponov et al., 1965

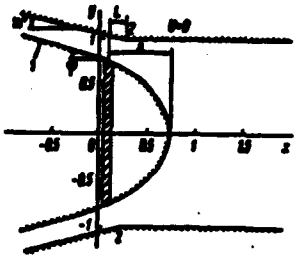

b) First Reported Gun Analysis by Lygin & Tsimring, 1972

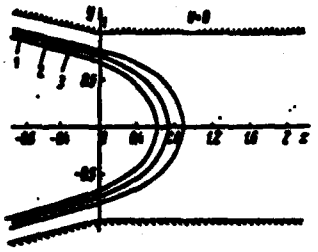

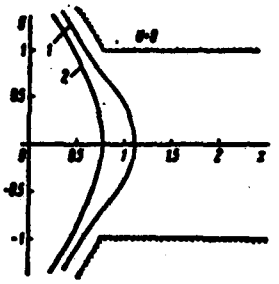

c) Guns using Anodes with Sharp Corners, Lygin & Tsimring, 1972

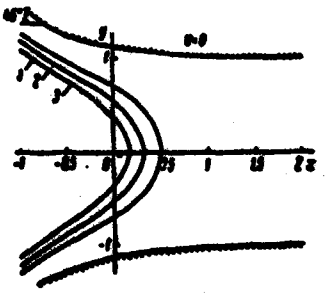

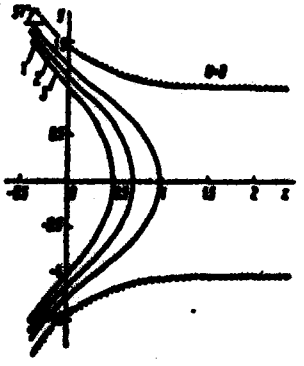

d) Guns with Smoothly Varying Anodes, Lygin & Tsimring, 1972

FIGURE A-1 - EARLY SOVIET EXPERIMENT AND GUN ANALYSIS

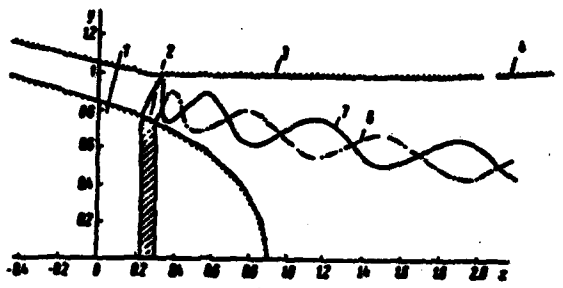

a) Electron gun for producing helical beams, and electron trajectories in gun with an anode angle.

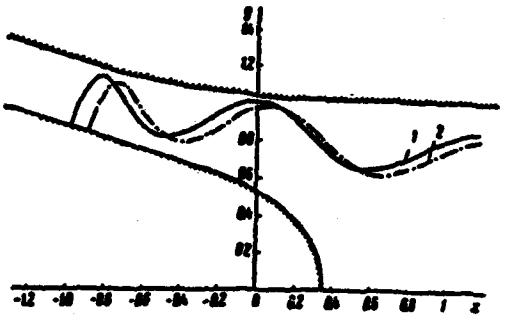

b) Electron trajectories in a gun with a smooth electrode configuration.

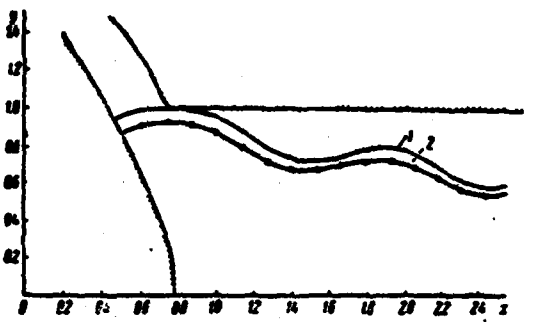

c) Electron trajectories in a gun in which there is a large angle between the cathode surface and the magnetic field.

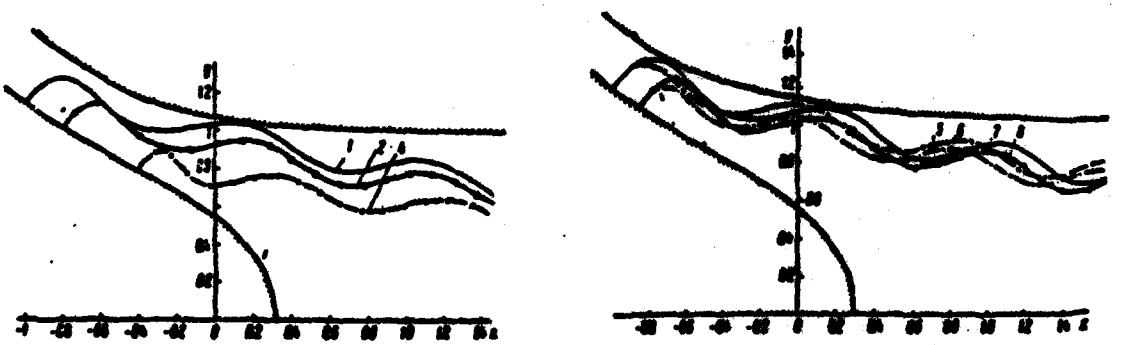

d) Electron trajectories in a gun with smooth electrode configurations.

FIGURE A-2 – FIRST REPORTED ELECTRON TRAJECTORY ANALYSIS BY LYBIN AND TSIMRING, 1972 (Ural paper).

2. Velocity Spread Analysis and Measurement

Tsimring, 1972, made a complete list of the variables which enter into velocity spread in MIG guns as follows:

1. Spread of the initial electron velocities.
2. Roughnesses of the emitting surface.
3. Violations of axial symmetry of the electric and magnetic fields.
4. The presence of nonuniform axisymmetric fields on the cathode, which are determined by the geometry of the gun electrodes and of the magnetic system.
5. Nonadiabatic fields in the intermediate region between the cathode and the second anode.
6. The space-charge field of the beam.

Of these variables, he states that in practice the only two whose effects cannot be reduced to arbitrarily small values (assuming small space-charge effects) are the first two. He then gives an analysis of the effects of initial electron thermal velocity spread and cathode surface roughness. These effects are described by the following two equations giving $\delta v_{\perp i}$, the fractional transverse velocity spread due to initial velocity spread at the cathode; and $\delta v_{\perp r}$, that due to cathode surface roughness. ($\delta v_\perp$ is defined as $2(v_{\perp 2} - v_{\perp 1})/(v_{\perp 2} + v_{\perp 1})$).

$$\delta v_{\perp i} = 3.6n \left(\frac{kT}{eV_a}\right)^{1/2} \left[\frac{d}{h}\left(1 + \frac{\pi^2}{4}\tan^2\phi\right)\right]^{1/2} \qquad (1)$$

$$\delta v_{\perp r} = 1.6n \left[\frac{r_o}{h}\left(1 + \frac{\pi^2}{4}\tan^2\phi\right)\right]^{1/2} \qquad (2)$$

Here, n is a velocity spread reduction factor due to interception of some fraction of the beam current on the anode.

$$n = 1 - 1.25\,(I_A/I_o)^* \qquad (3)$$

where I_A/I_o is the ratio of the anode to cathode current and is restricted to $I_A/I_o < 0.2$. The remaining variables are as follows: T is the cathode temperature in degree Kelvin; V_a is the anode voltage in volts; d is the cathode-to-anode separation, r_o is the cathode roughness (radius of a small hemisphere on the surface), h is the height of the first electron orbit, and ϕ is the angle between the cathode surface and magnetic field

---

* This function is an approximation to Tsimring's plotted function when intercepted current on the first anode is small.

at the cathode. This angle is restricted to <15° in the equations given. Note that the spread due to surface roughness is independent of anode voltage whereas that due to initial velocity varies as $V_a^{-1/2}$.

Based on equations (1) and (2), Tsimring concludes that the minimum transverse velocity spread due to cathode temperature alone for a 1000°K emitter temperature and a 10 kV anode voltage is approximately 1%. It is claimed, however, that a substantial additional velocity spread can occur due to the inherent surface physics of various types of cathode materials. Specifically, oxide cathodes are claimed to have initial energies up to 10 eV (Russian reference cited) which would produce up to 14% transverse velocity spread in a 10 kV gun and up to 5% spread in a 70 kV gun. For low velocity spread guns, this is a factor which needs to be evaluated.

Equation (2) above comes from Tsimring's analysis of the velocity spreading effects of a small hemispherical bump on the cathode surface. By direct analytic solution for the electric field distribution in the vicinity of the hemisphere and analysis of the spread in velocities of electrons which start with zero velocity on its surface, he concludes that a surface roughness of 2 μm can produce a transverse velocity spread of up to 5% independent of the beam voltage. This is a substantial factor and is the reason for the surface smoothness specification applied to NRL gun procurements.

It appears that an important part of any U.S. program to produce very low velocity spread guns for gyro-TWT applications must include direct measurements of the velocity spread produced by the cathode effects described above as well as the effects of other variables given in the previous list. A technique used extensively in the U.S.S.R. for velocity spread measurements was introduced and analyzed by Tsimring and is illustrated in Figure A-3. Its principle of operation is to longitudinally decelerate the beam by a variable retarding potential at the collector "5" which is placed in the working (peak magnetic field) region of the tube, and is used to measure the collected current as a function of retarding potential. Figure A-3(b) illustrates how the collected current is related to the longitudinal velocity distribution function.

The actual implementation and test results of a retarded potential beam analyzer are given in a pair of papers by Avdoshin et al. (April 1973) and Avdoshin and Gol'denberg (October 1973). Figure A-4 from the first paper shows the added electrodes required to implement the beam tester. The structure labeled "6" in Figure A-4(a) is the same as structure "1" in (b). This element is an "iris with sectional slits" and has the stated purpose of collecting the electrons which are reflected from the retarded potential on the collector. Collection takes place because the reflected electrons tend to be rotated in azimuth angle due to the crossed electric and magnetic field and therefore are collected by the blocked portions of the sectorial iris. If the electric field due to space-charge in the collector region is not sufficient to accomplish this rotation, an electron which returns to the gun acceleration region will be rotated and subsequently will have a high probability of interception as it is again accelerated toward the collector. The purpose of this electrode, then, is to prevent a large buildup of spacecharge which would disturb the measured beam.

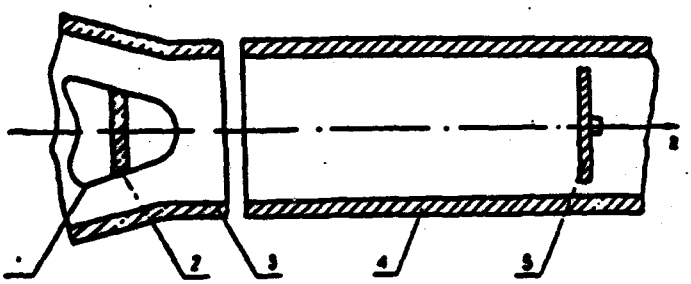

Diagram of the magnetron-injector adiabatic electron gun.

a) 1 is the cathode; 2 is an emitting strip; 3 is the first anode; 4 is the second anode; 5 is the collector which has a variable retarding potential.

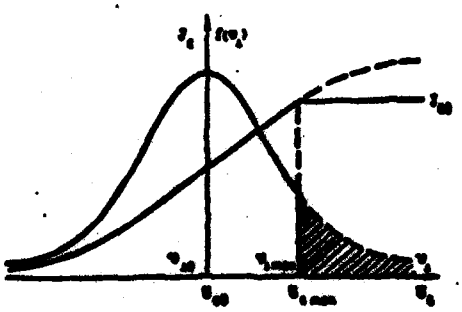

b) Distribution function over the oscillator velocities, and the collector-current cutoff curve for $J_e/J_0 \neq 0$.

FIGURE A-3 - FIRST DESCRIPTION OF VELOCITY SPREAD MEASUREMENT TECHNIQUES, TSIMRING, 1972

a)

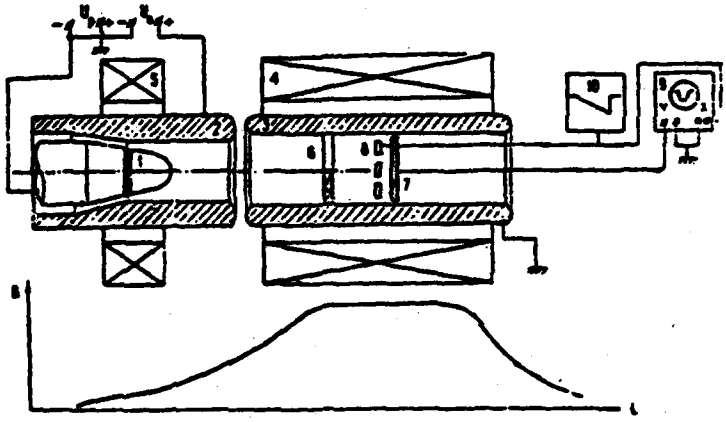

Diagram of the experimental installation for measuring the velocity spread. The axial distribution of the magnetic field is shown at the bottom.

b)

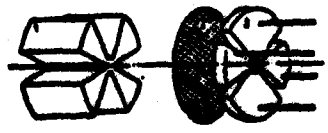

Elements of the velocity-spread analyzer: 1) iris with sectoral slits; 2) antidynatron grid; 3) sectioned collector.

FIGURE A-4 - EXPERIMENTAL DEVICE FOR VELOCITY SPREAD MEASUREMENT, AVDOSHIN, ET AL., APRIL, 1973.

The second added electrode is the "antidynatron grid" shown as structure "8" in Figure A-4(a) and "2" in (b). This mesh grid serves as the primary retarding element in the device and is swept in voltage as shown in the illustration of the oscilloscope test setup. Its major function is to prevent an erroneous measurement of collector current due to secondary emission of electrons which, without the grid, would be accelerated back toward the gun. Because the electron yield in secondary emission normally exceeds 100%,* for a metal collector and energies over 200 eV, it is conceivable that a reverse current flow or "dynatron effect" could result. The actual collector (structure "7") is held at a near ground potential in the measurement system so that all beam electrons which have sufficient velocity to pass through the retarding grid are accelerated toward the collector. Note in Figure A-4(b) that the collector "3" has also been sectioned to correspond with the iris. This permits independent measurements on the sampled portion of the beam and gives a gross indication of azimuthal uniformity in the beam.

It is interesting to note that the transverse velocity spread can be calculated to a good approximation directly from the electrode voltages in Figure A-4(a). For small spreads and weakly relativistic beams, the velocity spread is given by.

$$\frac{\Delta v_\perp}{v_\perp} \approx \frac{V_{g2} - V_{g1}}{2(V_0 - V_g)}$$

where $v_\perp/v_\perp$ is the fractional velocity spread in the transverse velocity, V_{g2} and V_{g1} are the retarding grid voltages at selected critical points which define the desired spread measurement (the Soviets use the 90% and 10% collector current points), V_0 is the beam voltage, and V_g is the mean voltage at which collector current cutoff occurs. It is relatively easy to verify that this equation is true by substituting the appropriate $v_z^2 = v_0^2 - v_\perp^2$ for the different voltages in the equation and reducing the result to $(v_{\perp 1} - v_{\perp 2})/v_\perp$. The velocity spread measurement is thus easily accomplished by monitoring the collector current and electrode voltages..

The primary results of the tests described by Avdoshin, et al., April 1973, are summarized in Table A-1. Five different cathode types with varying surface roughness were measured. Table A-1(a) shows that total velocity spreads in the range of 9 to 17% were obtained. Table A-1(b) gives a detailed description of the cathodes used including information on the materials and the construction technique. Cathode #5 is similar to the type-B matrix cathode used in the U.S.

The separate components of velocity spread due to surface roughness $\delta v_{\perp r}$ and initial velocity spread $\delta v_{\perp i}$ as shown in Table A-1(a) were calculated from equations 1 and 2. Because $\delta v_{\perp i}$ is the only component which depends on anode voltage, it is possible to experimentally verify the contribution of this component by measuring the reduction in $\delta v_\perp$ with increasing anode voltage.

---

* Walter H. Kohl, Electron Tubes, Reinhold Pub. Co., New York, 1960, p. 160.

	Cathode Type	Height of Roughnesses, r_0, μ	$\delta v_{\perp}$ exp %	$\delta v_{\perp r}$, %	$\delta v_{\perp i}$, %	Comments
1a	Yttrium oxide	20	17 ± 2	11	4	Grain size of the spongy material 20μ
1b	Yttrium oxide	25	17 ± 2	12	4	Grain size of the spongy material 40μ
1c	Yttrium oxide	10	14 ± 2	8	4	Spongy material smoothed
2	"Kerite" cathode	5	9 ± 1	5.5	4	Cathode ground
3	Oxide	5	17 ± 2	11	3	
4	Pressed oxide	5	9 ± 1	5.5	3	
5	Tungstate	5	9 ± 1	5.5	3	

(a)

1) An Yttrium Oxide Cathode. The working temperature was 1400-1600°C. The core material was molybdenum. A spongy material consisting of tantalum powder having a grain size of up to 40 was sintered with the core. After sintering an yttrium oxide Y_2O_3 powder was deposited on the spongy material. The samples of yttrium oxide emitters that were used had roughness dimensions of 20 to 25 and 10μ (in the latter case special mechanical treatment was used).

2) A Pressed Yttrium Oxide Cathode (a "Kerite" Cathode). The working temperature was 1600°C. The emitter was pressed in the shape of a washer consisting of a mixture of W (94%) and Y_2O_3 (6%). The grain size of the W was 2 to 3μ, and it was sintered at t = 2000°C. The height of the roughnesses was 5μ.

3) A Sintered Barium Oxide Cathode. The working temperature was 1000-1200°C. The surface space was approximately the same as it was for the yttrium oxide cathode.

4) A Pressed Oxide Cathode. The working temperature was 1100°C. The composition was 90% Ni and 10% basic barium-strontium-calcium carbonate. The plasticizer was polyvinyl alcohol; the molding pressure was 6 to 8 tons/cm^2. Sintering was carried out at t = 1200°C. The height of the roughnesses of the cathode surface was ~5μ.

5) A Tungstate Cathode. The working temperature was 1300°C. The composition was 90% W, 9% barium-calcium tungstate and 1% Al with an admixture of paraffin as a plasticizer. The molding pressure was 10 to 20 tons/cm^2. The sintering temperature was ~1800°C. The height of the roughnesses was ~5μ.

(b)

TABLE A-1. Summary of Measured Velocity Spreads for Several Different Type Cathodes; Avdoshin, et al., April 1973.

An example of such a measurement for the "kerite" cathode is shown in Figure A-5(a). This measurement was carried out in an operating mode in which the first orbits of the electrons were very close to the anode. This condition was maintained by keeping the ratio of the anode voltage to the square of the magnetic field at the cathode (V_a/B_c^2) constant.

The figure shows the measured velocity spread as a function of V_a (i.e., $U_a(V)$ in the figure). The authors state that the velocity spread components are statistically independent and therefore additive,* and utilizing equation (1), this data gives a cathode temperature of 1800-2000°K and component values of $\delta v_{\perp r} = 5.5\%$ and $\delta v_{\perp t} = 4\%$. The consistency of the results with the total measured velocity spread is excellent.

Figure A-5(b) shows the measured dependence of the transverse velocity spread on the intercepted anode current. This measurement was made by slightly changing the magnetic field at the cathode which changes the initial trajectories of the electron orbits, resulting in a change in the intercepted beam current. It is interesting to note that a rapid drop in the velocity spread occurs for a small amount of intercepted current. Avdoshin, et al. (April 1973) noted that these results are "evidence of the expediency of using precritical operating modes of the gun" in which that portion of the beam with excess transverse velocities is collected on the first anode.

Although a significant velocity spread reduction of several percent was achieved for an anode intercepted current of only 2% (as shown in Figure A-5(b)), the merits of this approach are open to question and need further investigation. For example, the change in velocity spread is strongly dependent on the definition of the spread. In the case shown, apparently only a very small portion of the beam was involved in the excess spread and therefore it conceivably would have very little effect on the rf interaction anyway.

The general idea of using mechanical filtering techniques for velocity spread reduction, however, deserves further investigation. For example, it may be possible to use a selective aperture to eliminate undesirable portions of an electron beam which have divergent characteristics due to space-charge or fringing fields. Such an aperture could conceivably be at a low potential with respect to the cathode (thus limiting the power dissipation) and could serve a dual role as a modulating electrode.

The final velocity spread measurements reported by Avdoshin et al. (April 1973) and Avdoshin and Gol'denberg (October 1973) are shown in Figure A-6. The first two figures, A-6(a) and (b), show the measured velocity spread dependence on beam current (expressed as a fraction of the theoretical space-charge limited current in Figure A-6(a). Data from four different type cathodes are shown, and in all cases, the velocity spread is an increasing linear function of the cathode current.

This linear increase in velocity spread with beam current was derived theoretically by Gol'denberg and Petelin (1973) for adiabatic MIGs. The cathode configurations used in this analysis are shown in Figure A-7 and

---

* We question this since standard deviations usually are squared and added (i.e., the variances are additive).

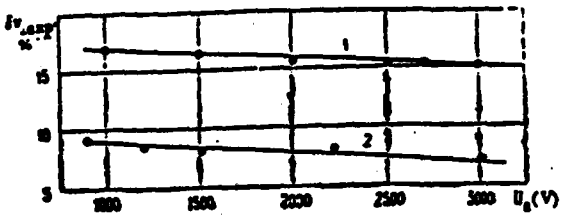

(a)

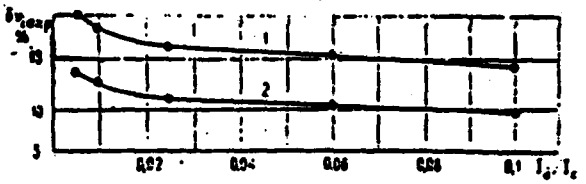

(b)

FIGURE A-5 - MEASURED VELOCITY SPREAD AS A FUNCTION OF (a) ANODE VOLTAGE AND (b) ANODE CURRENT FOR (1) THE "YTTRIUM OXIDE" CATHODE AND (2) THE "KERITE" CATHODE.

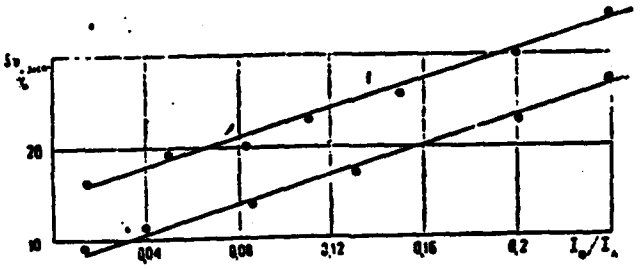

a) Avdoshin et al., April, 1973

Dependence of the spread of the oscillator velocities on emission current: 1) yttrium oxide cathode; 2) "kerite" cathode.

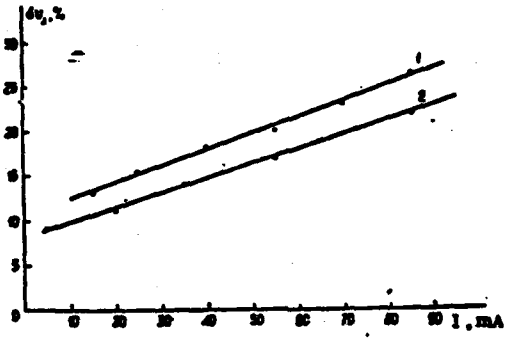

b) Avdoshin and Gol'denberg, October, 1973

Dependences of the scatter of the oscillator velocities of the electrons on emission current: 1) scintered cathode; 2) pressed cathode.

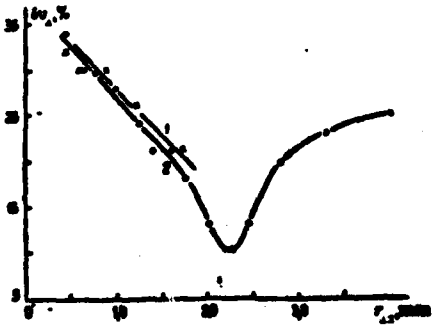

c) Avdoshin and Gol'denberg, October, 1973

Dependences of the scatter of the oscillator velocities of the electrons on the rotation radius of the electron in the injector for guns differing in the magnitude of the gap d between the anode and cathode; 1) d = 3.5 mm; 2) d = 8 mm.

FIGURE A-6 - MEASUREMENTS OF TRANSVERSE VELOCITY SPREAD AS A FUNCTION OF BEAM CURRENT AND CATHODE FIELDS WITH DIFFERING CATHODE TYPES AND ELECTRODE SPACING.

a)

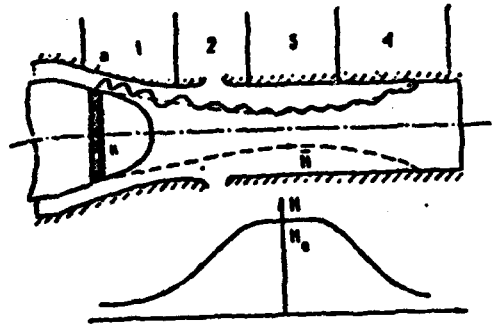

The electron-optical system of the CRM. 1) Injector (a is the anode and k is the cathode); 2) magnetic-reversal region; 3) working space of the CRM; 4) collector. The magnetic field distribution along a system axis is shown in the bottom graph.

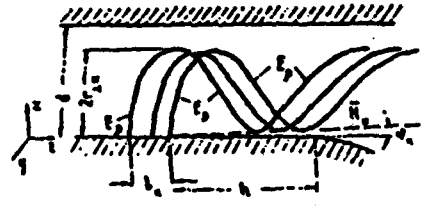

b)

An adiabatic gun with a narrow emitter.

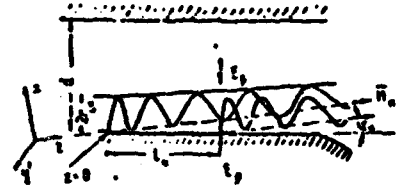

c)

An adiabatic gun with a wide emitter.

FIGURE A-7 - THEORETICAL SPACE-CHARGE EFFECTS IN ADIABATIC MIGs. GOL'DENBERG AND PETELIN, 1973.

their results are claimed to be applicable for either narrow or wide emitting strips in the gun. One of their conclusions is that due to increasing velocity spread, a limiting current exists for these type MIGs and that its value is the same for either narrow or wide cathodes. This is a surprising result, but it must be kept in mind that it applies only for an adiabatic gun, and non-adiabatic trajectories may greatly change this conclusion.

For the purpose of low-velocity-spread design work, the measurement shown in Figure A-6(c) re-emphasizes the fact that the detailed shape of the electron orbits in the vicinity of the cathode can have dramatic effects on the velocity spread, and that the velocity spread can have a strong minimum with respect to the first orbit radius, $r_\perp$ ($r_\perp$ varies as $V_a^{1/2}/B_c$ at the cathode). The figure also shows that the spread is not a function of the distance to the first anode, although if the distance is too short, it may not be possible to reach the minimum due to anode interception.

The explanation given for this behavior is that the variation of $r_\perp$ at the cathode carries the electron trajectories through different parts of the cathode "fringing field" (i.e., the transition region where the electric field changes from predominantly transverse to longitudinal in direction). The conclusion is that "electron-optic systems in which the electrons travel in the fringing field of the cathode with approximately identical rotation phases along trajectories that are furthest from the end of the cathode are preferable." In other words, if possible, it is best to form a beam in which all of the electrons have the same spatial phase and follow the most adiabatic path through the transition region of the gun.

The sharpness of the velocity spread minimum in Figure A-6(c) indicates another important fact for experimentally adjusting a MIG gun. It shows that values of $\sqrt{V_a}/B_c$ at the cathode should be thoroughly and carefully explored for any given gun configuration to make sure that operation at the velocity spread minimum has been achieved.

In 1975 Antakov, et al., published the results of extended velocity spread measurements on a 16 kV two-electrode gun using the decelerating field method described above. No diagram of the gun configuration was given but the gun was described as having a narrow cathode emitting strip (surface area = 2 cm^2) whose width was much less than the 0.8 cm cathode-anode spacing. Also, the cathode electrode was mounted so that the electrode could be moved both longitudinally and transverse to the gun axis to measure the effects of misalignments. The measurement results are shown in Figure A-8.

Figure A-8(a) shows both the velocity spread $\delta v_\perp$ and the transverse to longitudinal velocity ratio "g_0" = $v_\perp/v_z$ as functions of the beam current normalized to the space-charge limited "Langmuir" current, I_0/I_ℓ ($I_\ell \cong 20A$). The parameter "α" shown in the figure is the ratio of the interaction magnetic field to the cathode magnetic field (B_0/B_c). Note that the transverse velocity spread is the same for all values of B_0/B_c as required by the theory

---

* To maintain consistency with Figure 8 and following figures in this Appendix, which have been reproduced from a prior report, the symbol for the Langmuir current is "I_ℓ", not "I_L" as in the body of the main text.

a)

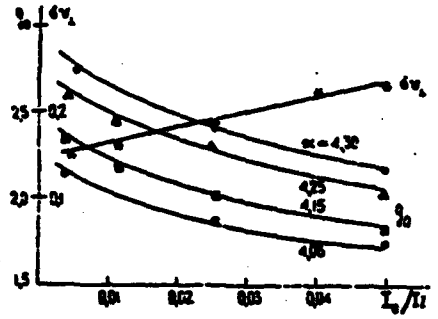

b)

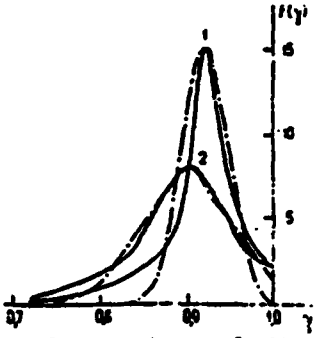

Measured values of g_0 and $\delta v_\perp$ and comparison of experimental distribution functions for transverse velocities (solid curve) with an approximating Gaussian function (dashed-dot curve) for $\alpha = 4.25$ (1 is for $I_0/I_\ell = 2.5 \cdot 10^{-2}$, 2 is for $I_0/I_\ell = 5 \cdot 10^{-2}$).

c)

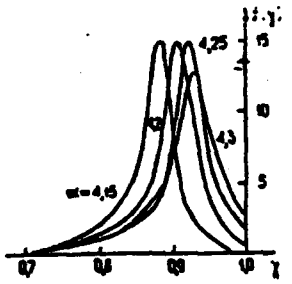

d)

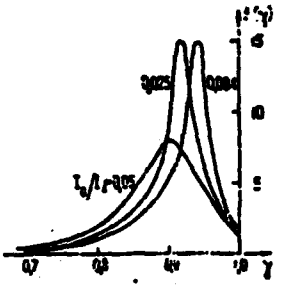

Evolution of electron-velocity distribution function for variation c) of the magnetic reversal α, ($I_0/I_\ell = 2.5 \cdot 10^{-2}$; d) of the electron-beam current ($\alpha = 4.2$).

e)

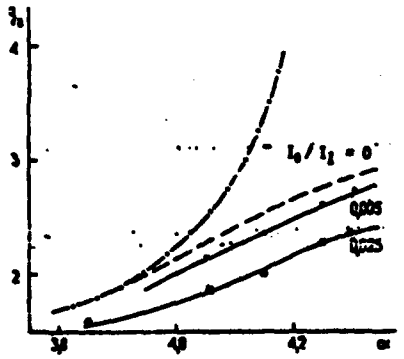

f)

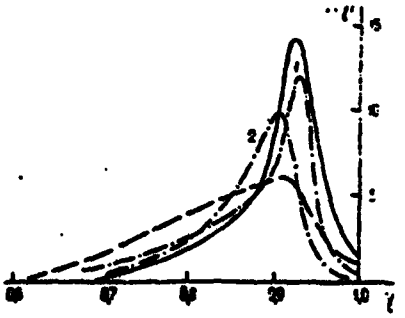

e) Comparison of the theoretical (dashed-dot) and experimental (split) curves for the dependence of g_0 on the magnitude of the magnetic reversal α. The dashed curve was obtained by extrapolating the experimental data into the region of low currents ($I_0/I_{\ell\,0}$).

f) Distribution of electron velocities for various positions of the cathode ($\alpha = 4.25$, $I_0/I_\ell = 2.5 \cdot 10^{-2}$; the solid curve is for the optimal cathode position the dashed curve is for displacement of the cathode by 0.1 d in the radial plane; the dashed-dot curve is for displacement of the cathode along the gun axis; 1) $z = 1.5\ell_c$, 2) $z = -1.5\ell_c$).

FIGURE A-8 - BEAM MEASUREMENTS ON A MAGNETRON INJECTION GUN BY ANTAKOV, ET. AL., (1975). DEFINITIONS: $\alpha = v_\perp/v_0$, $g_0 = v_\perp/v_z$, $\alpha = B_0/B_c$, $\delta v_\perp = (v_{\perp 2} - v_{\perp 1})/v_\perp$, $f(\alpha)$ = VELOCITY DISTRIBUTION FUNCTION I_0/I_ℓ = NORMALIZED BEAM CURRENT. SEE TEXT FOR DETAILED EXPLANATION.

of adiabatic guns. Two of the corresponding velocity spread distribution functions ($f(\gamma)$ obtained by differentiating the measured current shut-off characteristics are shown in Figure A-8(b). These two curves (solid lines) are functions of "γ" = $v_\perp/v_0$ and were taken for $B_0/B_c = 4.25$ and two currents: (1) $I_0/I_\ell = 0.025$ and (2) $I_0/I_\ell = 0.05$. The dashed-dot curves represent Gaussian distribution functions which are fit to the two measured distribution functions. Note that the distributions in this case are fairly well represented by Gaussian curves except in the low transverse velocity region. In this region where measurements require that most of the beam be reflected, the authors state that some difficulties were encountered with the measurement system because of the increased space-charge of the reflected beam. The actual existence of the long tail of high longitudinal velocity electrons is therefore questionable.

Figures A-8(c) and (d) give parametric variations of the transverse velocity distribution functions. Figure A-8(c) shows the variation with magnetic compression B_0/B_c when $I_0/I_\ell = 0.025$, and Figure A-8(d) shows the variation with I_0/I_ℓ when $B_0/B_c = 4.2$. In both cases, the peaks of the distribution functions shifted; but only in the case of increasing I_0/I_ℓ did they get wider (more spread).

Figure A-8(e) shows the variation of $v_\perp/v_z$ versus B_0/B_c with I_0/I_ℓ as a parameter. The fairly strong discrepancy between the measured curves and the theoretical dash-dot curve is explained on the basis of space-charge depression in the cathode region due to reflection of the high transverse velocity tail from the magnetic mirror when $B_0/B_c > 4.15$ (see Figure A-8(c)) or due to high current $I_0/I_\ell \gtrsim 0.025$. The theory and experiment in this case only agree for $I_0/I_\ell \cong 0$ and $B_0/B_c \lesssim 4.0$ ($v_\perp/v_z \lesssim 2$). The significance for gun design purposes is that when $v_\perp/v_z \gtrsim 2$, one must begin to expect strong space-charge effects in the gun due to current in the tail of the velocity distribution function being reflected from the magnetic mirror.

The last figure, A-8(f), shows the effects on velocity distribution due to errors in the cathode electrode position. The solid curve is the distribution function for optimal placement, the dash-dot curves (1) and (2) resulted when the cathode was pushed forward and backward by 1.5 cathode widths, respectively, and the dashed curve resulted from a transverse shift of 10% of the anode-cathode gap. All of these displacements are rather severe in terms of mechanical errors, but they do emphasize the need to understand displacement tolerances in these guns. The transverse misalignment appears not only to be the most critical, but the most likely to occur considering that the cathode electrode requires a cantilevered construction and a large temperature differential. This is especially true for very small guns required at short millimeter wavelengths.

Overall, the series of Figures A-8(a) through (f) represent the kind of data which needs to be obtained on MIGs now being used in the U.S. The lack of such measured data has not only made the results of rf experiments hard to interpret, but has precluded an accurate calibration of the computer simulation tools used for gun design in this country.

3. Synthesis of High Power Gyrotron Guns

Probably the most significant Soviet work to date with respect to high power gyrotron guns is published in a pair of relatively recent papers by Tsimring (1977) and Manuilov and Tsimring (1979). In these two papers, Tsimring and Manuilov have extended the theory of the planar MIG (Kino and Taylor, 1962) and the cylindrical MIG (Dryden, 1962; and Harker, 1960/62/63) to include the effects of temperature limited operation and beams with large transverse energy. This extended theory was required because the original MIG theories were aimed at producing laminar flowing beams from space-charge limited cathodes. A new space-charge parameter is defined by Tsimring as

$$\text{"}\gamma\text{"} = \frac{j_c}{\epsilon_0 \omega_c E_c}$$

where j_c is the cathode current density, E_c is the electric field at the cathode, and ω_c and ϵ_0 are the cyclotron frequency at the cathode and the permittivity of free space, respectively. The parameter "γ" then varies from zero (no space charge) to infinity ($E_c = 0$ or fully space-charge limited).

Samples of the electron trajectories obtained from integrating Tsimring's equations of motion in a rectangular (normalized) cathode coordinate system are shown in Figure A-9(a). Tsimring points out that in order to achieve an analytical solution for the beam flow, it is necessary that the electron trajectories do not cross but maintain a laminar-like flow such as shown in the figure. This stipulation of laminar-beam-flow leads directly to a critical relationship between the angle ϕ of the magnetic field with respect to the cathode (see Figure A-9(b)) and the space-charge parameter defined above. This critical relationship is shown in Figure A-9(c). For values of ϕ above the line, laminar flow is obtained and for values below the line, the electron trajectories begin crossing.

Laminar flow is important in high density electron beams for another reason which was previously described (Gol'denberg and Petelin, 1973) and which Manuilov and Tsimring re-emphasize. When the electron trajectories cross and re-cross in an ordered set of intersections, the net result due to space-charge forces in the beam is to produce increasing velocity disparity between electrons emanating from opposite edges of the cathode. This results in a large velocity spread when the cathode electric field is depressed by as little as 10% from its zero space-charge value. When laminar flow is maintained, however, Tsimring states that depression of the cathode electric field can be as large as 50% without excessive velocity spread. This translates into greatly increased beam powers for gyrotron applications.

The principal effect of space-charge in laminar flow beams is to reduce the value of $v_\perp/v_z$ as beam current density is increased. This effect, however, unlike severe velocity spreading, does not preclude use of the beam in gyrotron applications. For example, a 30 kV, 70 A (2.1 MW) gun design cited by Tsimring had a value of $v_\perp/v_z = 0.9$ which is considerably lower than any used in experimental gyrotrons in the U.S. thus far.

To proceed with the synthesis of intense beam MIGs, Tsimring and Manuilov use the same techniques described in the cited planar and cylindrical MIG design literature. First, they solve the "internal" beam flow problem

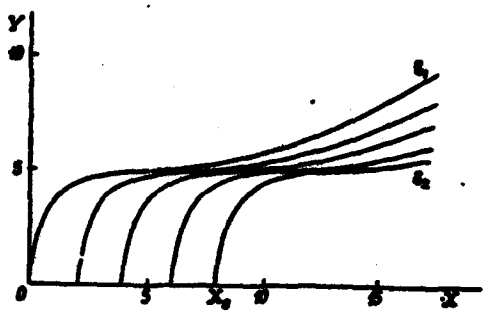

a) Electron trajectories in a plane with $\gamma = 0.5$ and $\phi = 15°$.

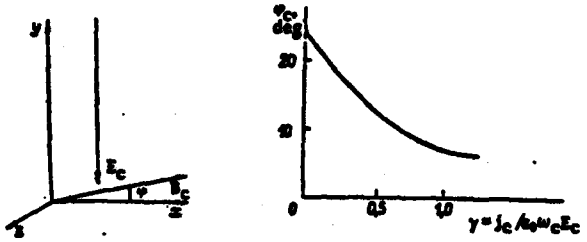

b) c)

b) Electric field and magnetic field at the cathode of a planar magnetron-injection gun.

c) Dependence of the critical inclination angle of the magnetic field to the plane of the cathode on the parameter γ.

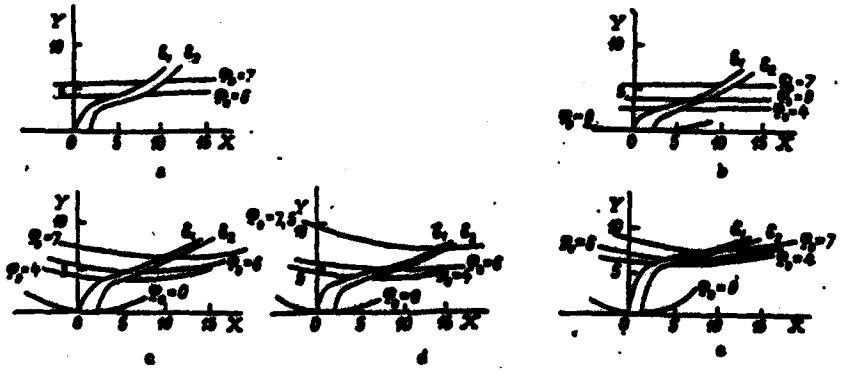

d)

d) Equipotential lines and trajectories in electron beams with various parameters: a) $\gamma = 0$, $\phi = 30°$; b) $\gamma = 0.1$, $\phi = 25°$; c) $\gamma = 0.3$, $\phi = 20°$; d) $\gamma = 0.5$, $\phi = 15°$; e) $\gamma = 1.0$, $\phi = 10°$ (ϕ_0 are the anode potentials).

FIGURE A-9 - DESIGN SYNTHESIS OF DENSE GYROTRON BEAMS FROM TSIMRING, 1977. LAMINAR FLOW (a) IS ACHIEVED FOR MAGNETIC FIELD ANGLES ϕGREATER THAN ϕc (b and c). THE EFFECT OF INCREASING THE SPACE-CHARGE PARAMETERS "a" IS SHOWN IN (d).

based on the differential equations of motion for an extended beam. They then find the potential along the two trajectories representing the two cathode edges, and through a conformal mapping of these trajectories to the axes of transformed coordinate system and an analytic continuation of the potential functions, they are able to determine the shape and position of the equipotentials outside of the beam. This is termed a solution to the "external" problem. Some typical results for rectangular MIGs are shown in Figure A-9(d).

The procedure required to utilize the solutions shown in Figure A-9(d) for MIG design is to set the cathode off axis at the required design radius, and to tilt it such that the slope of the magnetic field lines is zero or slightly downward. An equipotential line is then selected as the anode shape and at the point where the beam intercepts this equipotential, the anode shape is smoothly changed to prevent interception. This is illustrated in Figure A-10 (a, b and c). Figure A-10(b) is the result for low space-charge and (c) shows electrode shapes for moderately heavy space-charge.

The deviation of the anode shape from the calculated equipotential line is stated to have only a small perturbing effect if it occurs well away from the cathode so that the cathode electric field is undisturbed, and if it is done smoothly enough to preserve adiabatic flow. Tsimring notes that, in any case, this synthesis process must be backed up and verified and perhaps optimized by a computer simulation which includes the effects of space-charge. The synthesis procedure thus provides the starting point for the computer analysis-optimization procedures.

The most recent paper by Manuilov and Tsimring (1979) describes what appears to be very important gun design tools which should be understood, verified, and utilized in the U.S. gyrotron program. In this paper, the MIG beam is described in terms of a modified Dryden flow (Dryden, 1962) in cylindrical geometry. The solutions for the laminar trajectories and the internal and external potentials are carried out simultaneously using a computer code in which the conformal mapping and analytic continuation procedures have been completely automated.

In order to extend the theory to cylindrical geometry, a new "cylindricity" parameter μ was defined as

$$\mu = \frac{E_c}{\eta B_c^2 r_c}$$

where E_c and B_c are the electric and magnetic fields at the cathode and r_c is the cathode radius. The constant η is the charge to mass ratio for electrons. The parameter μ is essentially just the ratio of the Larmor radius to the cathode radius and when it approaches zero, the trajectories from a cylindrical cathode are very close to those from a rectangular geometry cathode with the same cross-sectional dimensions. In fact, the cylindrical theory given approaches Tsimring's rectangular theory as μ approaches zero.

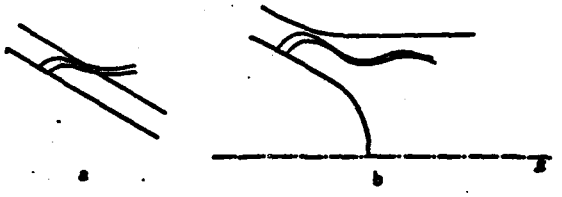

Correction of the electrodes in an electron gun with a weak shape-charge: a) original shape; b) final shape.

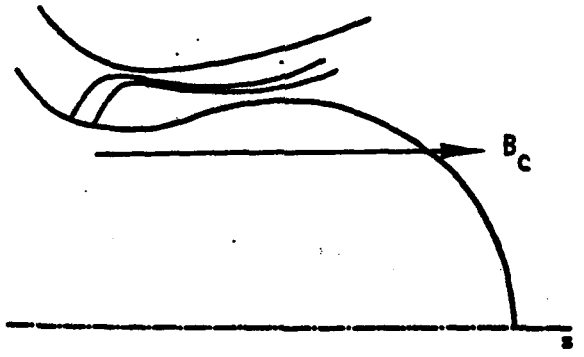

Electrode configuration in an electron gun with $\gamma = 0.5$ and $\phi = 15°$.

FIGURE A-10 - MIG ELECTRODE SHAPES FROM TSIMRING, 1977.

There are two important differences between the cylindrical MIG theory and the rectangular theory. First, the critical magnetic field angle which separates laminar flow from crossed trajectory flow becomes a function of both the space-charge parameter "γ" and the cylindricity parameter μ. This is shown in Figure A-11(a) (compare Figure A-9(c)). Note that determining a value for the magnetic field angle is much more complicated in the cylindrical case. In general, Manuilov and Tsimring suggest that small angles are best because this leads to larger rotational velocities (larger $v_\perp/v_z$) and smaller positional velocity spread (i.e., spread caused by widely separated cathode trajectories). With respect to the latter advantage, they point out that for an adiabatic gun, the velocity spread between electrons leaving opposite edges of the cathode is given by

$$\delta v = \ell_s \sin \phi_c$$

where ℓ_s is the cathode slant length and ϕ_c is the magnetic field angle with respect to the cathode.

The second important difference is that in the cylindrical case, the beam reaches a maximum potential when μ is greater than 0.05. An example of this is shown in Figure A-11(b). The importance of this fact is that an anode potential can be selected above the maximum potential in the beam and the resulting anode shape does not have to be arbitrarily altered to prevent beam interception. The result should be a much closer correspondence between the theory and experiment in guns with this characteristic. Note in the figure that dashed curves showing the corresponding beam and equipotential from the rectangular geometry theory are shown for comparison.

In summary, over a period of more than 15 years, the Soviets appear to have done a rather thorough job of examining the theory and techniques required to design and build MIG type guns for gyrotron devices. Most of the design criteria used in the U.S. has been picked up from this literature in a somewhat piecemeal manner as needed. Successes in U.S. gun designs have been mainly the result of using large-scale gun simulation computer codes to refine and optimize designs based on simple adiabatic design criteria. It is now evident that additional work is needed to understand and implement design theory and analysis similar to that published by Tsimring and Manuilov. This type of theoretical insight and understanding will be required as the demand for higher beam powers and lower velocity spreads continues. It is also evident that direct measurements of gyrotron beam parameters and velocity spread such as those carried out by the Soviets will be required to establish the effectiveness of our design tools.

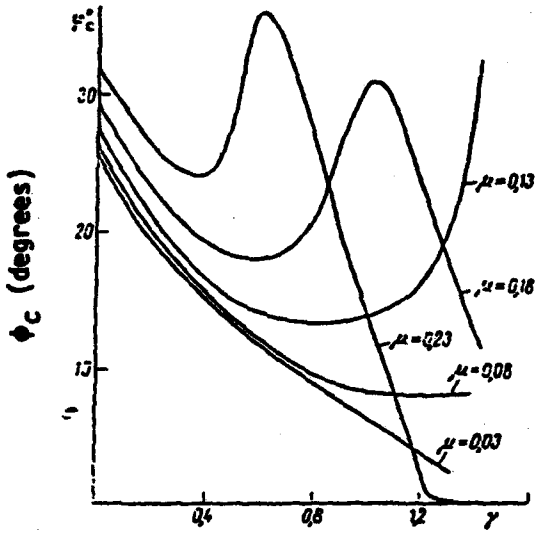

a) Dependence of the critical cathode angle on the space-charge parameter.

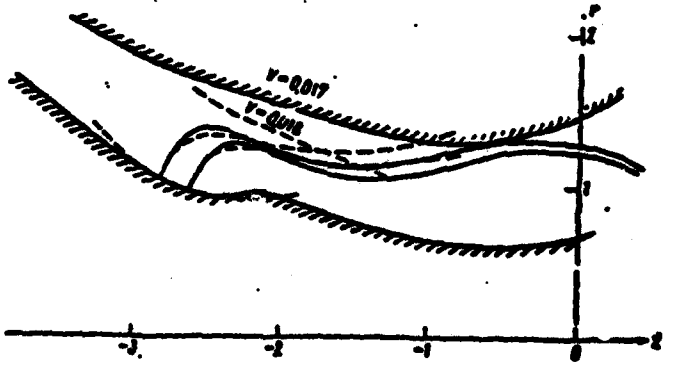

b) Shape of electrodes and trajectories in a system with $\mu = 0.10$. Dashed-planar model ($\mu = 0$).

FIGURE A-11 - CYLINDRICAL MIG DESIGN: (a) CRITERIA FOR LAMINAR FLOW ($\phi > \phi_c$), and (b) ELECTRODE DESIGN FROM RAMUILOV AND TSIMRING, 1979.

AD-A119 707 B-K DYNAMICS INC ROCKVILLE MD F/G 9/1
GYROTRON GUN STUDY REPORT.(U)
SEP 81 J M BAIRD, A C ATTARD N000173-79-C-0132
UNCLASSIFIED TR-3-476 NL

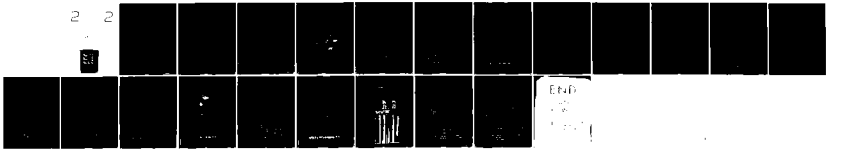

APPENDIX B

ELECTRON EQUATIONS OF MOTION AND BEAM GEOMETRY RELATIONSHIPS

APPENDIX B

ELECTRON EQUATIONS OF MOTION AND BEAM GEOMETRY RELATIONSHIPS

The equations of motion for relativistic electrons traveling in time independent electric and magnetic fields which are cylindrically symmetric can be obtained in cyclindrical coordinates (r, θ, z) from the Lagranian function*

$$L = -m_0c^2 \left[1 - (\dot{r}^2 + r^2\dot{\theta}^2 + \dot{z}^2)/c^2\right]^{1/2} + e\Phi - er\dot{\theta}A_\theta \qquad \text{(B-1)}$$

where m_0 is the rest mass of electrons, c is the velocity of light, e is the magnitude of the electronic charge, $\Phi(r,z)$ is the electric potential, and $A_\theta(r,z)$ is the magnetic potential. Dots are used to indicate the total derivative with respect to time, and mks units are used throughout.

The equations of motion are given by

$$d/dt\ [\partial L/\partial \dot{q}_i] - \partial L/\partial q_i = 0 \qquad \text{(B-2)}$$

For the three respective coordinates this gives

$$d/dt(m_0\gamma\dot{r}) - m_0\gamma r\dot{\theta}^2 - e\partial\Phi/\partial r + e\dot{\theta}\ \partial(rA_\theta)/\partial r = 0 \qquad \text{(B-3)}$$

$$d/dt(m_0\gamma r^2\dot{\theta} - erA_\theta) = 0 \qquad \text{(B-4)}$$

$$d/dt\ (m_0\gamma\dot{z}) - e\partial\Phi/\partial z + e\theta r\ A_\theta/\partial z = 0 \qquad \text{(B-5)}$$

It is immediately evident from equation B4 that regardless of the presence of an accelerating potential $\Phi(r,z)$ in a cyclindrical electron gun, the angular momentum is conserved so that

$$(m_0\gamma r^2\dot{\theta} - erA_\theta) = \text{constant of motion} \qquad \text{(B-6)}$$

---

* W. Rindler, Special Relativity, Interscience Publishers, Inc., New York, 1960, p. 106

To write this equation in terms of the magnetic field $\vec{B} = \nabla \times \vec{A}$, or

$$\vec{B} = (\hat{r}/r)\partial(rA_\theta)/\partial\hat{z} + (z/r)\partial(rA_\theta)/\partial r \qquad \text{(B-7)}$$

where $\hat{r}$ and $\hat{z}$ are unit vectors in their respective directions, we introduce the near axis approximation

$$A_\theta \simeq rB_z(z)/2 \qquad \text{(B-8)}$$

where $B_z(z)$ is the value of the magnetic field on the axis of the system. When Equation B8 is put into Equation B7, the result is

$$\vec{B} = (rB_z'/2)\,\hat{r} + B_z\,\hat{z} \equiv B_r\hat{r} + B_z\,\hat{z} \qquad \text{(B-9)}$$

where $B_z' = dB_z/dz$. The constant of motion (Equation B6) is thus

$$[\gamma r^2\dot{\theta} - (eB_z/2m_0)r^2] = \text{constant} \qquad \text{(B-10)}$$

Equation B10 provides a very useful relationship for gyrotron beam design if we evaluate r and $\dot{\theta}$ in terms of the geometric parameters in the gyrotron beam cross section shown in Figure B1. From the figure the vector relationship $\vec{r} = \vec{b} + \vec{a}$ gives

$$r^2 = b^2 + a^2 + 2ab\cos\phi \qquad \text{(B-11)}$$

If we divide the angle θ in the Figure into constant and time varying parts,

$$\theta(t) = \theta_0 + \theta_1(t) \qquad \text{(B-12)}$$

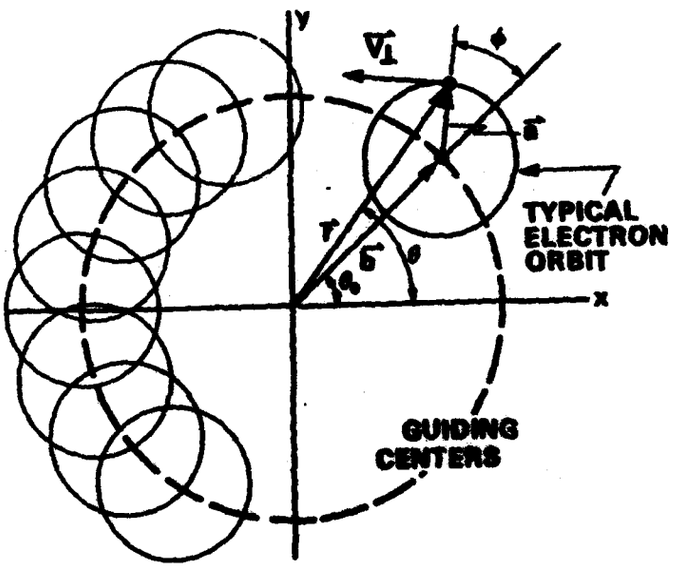
y
$V_\perp$
ϕ
$\vec{a}$
TYPICAL
ELECTRON
ORBIT
$\vec{r}$
$\vec{b}$
θ
θ_0
x
GUIDING
CENTERS

FIGURE B1

we see that $\dot{\theta} = \dot{\theta}_1$, where $\dot{\theta}$ can be obtained by differentiating

$$\tan \theta_1 = a \sin \phi/(b + a \cos \phi) \tag{B-13}$$

with respect to time. The result is

$$\dot{\theta}_1/\cos^2\theta_1 = [(a^2 + ba \cos \phi)/(b + a \cos \phi)^2]\dot{\phi} \tag{B-14}$$

Then, using $\cos \theta_1 = (b + a \cos\phi)/r$ and $\dot{\phi} = \omega_c$, we get from Equations B12 and B14

$$r^2\dot{\theta} = (a^2 + ba \cos \phi)\omega_c \tag{B-15}$$

Equations B11 and B15 then provide the means to evaluate the constant of motion in Equation B10. The result is

$$[\, r^2\dot{\theta} - (eB_z/2m_0)r^2] = eB_z/2m_0\ (a^2 - b^2) \tag{B-16}$$

where the cyclotron frequency ω_c has been replaced by $eB_z/m_0\gamma$ and B_z is the axial magnetic field at the position where the cross section shown in Figure B1 pertains.

If we now evaluate the lefthand side of Equation B16 at the cathode where $\gamma_c = 1$, $B_z = B_{zc}$, and $r = r_c$, and the right hand side in the rf interaction region, and if we assume that $\dot{\theta}_c = 0$ (assumes negligible transverse thermal velocity at the cathode), we get

$$B_{zc}r_c^2 = B_0(b_0^2 - a_0^2) \tag{B-17}$$

For ring cathodes such as those used in gyrotron Magnetron Injection Guns (MIGs), Equation B17 gives an extremely simple and important design relationship between cathode radius and cathode magnetic field. The equation holds for cylindrically symmetric beam forming systems regardless of beam acceleration and compression, and regardless of non-adiabatic effects. Note that the relationship between r_c and B_{zc} is fixed once the desired beam geometry and field in the rf interaction region are fixed, and that Equation B17 can be used as a design trade-off relationship in determining the size of the cathode required.

Equation B16 can be used to demonstrate several additional properties of cyclotron motion in beams. First, if the constant of motion is evaluated at two different points along a beam during magnetic compression we get

$$B_1(b_1^2 - a_1^2) = B_2(b_2^2 - a_2^2) \qquad \text{(B-18)}$$

which can be rearranged as

$$B_1 b_1^2 - B_2 b_2^2 = B_2 a_2^2 - B_1 a_1^2 \qquad \text{(B-19)}$$

It is easy to show that under adiabatic compression of the beam the right-hand side of Equation B19 is zero since Ba^2 is proportional to $\gamma^2 v_\perp^2/B$ which is conserved (conservation of magnetic moment). Thus,

$$b_1/b_2 = a_1/a_2 = \sqrt{B_2/B_1} \qquad \text{(B-20)}$$

where $\sqrt{B_2/B_1}$ is the magnetic compression factor for linear dimensions. This shows that a gyroton beam maintains its relative cross-section geometry under adiabatic magnetic compression.

A second interesting use for Equation B16 involves the non-adiabatic case of stepped magnetic fields.

Returning to Equations B8 and B9, it is easy to show that stepped fields also satisfy these relationships. A simple field step from B_1 to B_2, for example, can be described by

$$B_z(z) = B_1(1-u)+B_2u \qquad \text{B21}$$

where *

$$u(z) = \begin{cases} 0 & ; z < 0 \\ 1/2 & ; z = 0 \\ 1 & ; z > 0 \end{cases} \qquad \text{B22}$$

is the Heaviside unit step function. Useful relationships involving the derivative of u(z) are given by

$$\begin{aligned} du/dz &= \delta(z) = \text{Dirac delta function}^{**} \\ \int f(z)\delta(z)dz &= f(0) \\ \int u(z)\delta(z)dz &= u(0) = 1/2 \end{aligned} \qquad \text{B23}$$

For the stepped magnetic field given in Equation B21, it can be shown that the relationships between A_0 and B_z given by Equations B8 and B9 still hold true with B_r being a delta function. When this is followed through the derivation of equations B17 and B18, it is found that these equations are still valid. In equation B17, if there is no magnetic field at the cathode

---

* M. Abramowitz and I. A. Stegan, Handbook of Mathematical Functions, U. S. Government Printing Office, 1964, p. 1020.

** J. D. Jackson, Classical Electrodynamics, John Wiley & Sons, Inc., New York, 1962, pp 3-4.

so that $B_{zc} = 0$, then $b_o = a_o$ and upon entering a stepped magnetic field the electrons will oscillate through the z axis. Or, for field reversal where $B_{zc} = -B_o$ and $r_c = a_o$, equation B17 gives $b_o = 0$ so that the beam emerging from this field reversal spirals directly around the z axis at constant radius a_o.

The equations of motion can be put into a more useful form for beam analysis by assuming that the constant angular momentum of an electron is defined at its cathode origin by the equation

$$m_o\gamma_c r_c^2\dot{\theta}_c - er_c^2 B_{zc}/2 = -m_o\gamma_c r_c^2\Omega_c \qquad \text{(B24)}$$

which gives

$$\Omega_c = \omega_{tc}/2 - \dot{\theta}_c \qquad \text{(B25)}$$

where ω_{cc} is the cyclotron frequency at the cathode ($\omega_{cc} = eB_{zc}/m_o\gamma_c$). If we then assume that the trajectory proceeds through an acceleration region into a drift region where $\Phi = 0$ and A_θ is given by equations B8 in terms of B_z and r, the result is

$$\ddot{r} - r\dot{\theta}^2 + (e/m_o\gamma)r\dot{\theta}B_z = 0 \qquad \text{(B26)}$$

$$r^2\dot{\theta} - 1/2\,(e/m_o\gamma)r^2 B_z = -\Omega_c r_c^2 \qquad \text{(B27)}$$

$$\ddot{z} + 1/2\,(e/m_o\gamma)\dot{\theta}r^2 B_z' = 0 \qquad \text{(B28)}$$

where $B_z' = dB/dz$. These equations hold for any variation of the magnetic field for which equation B8 holds, including stepped fields (e.g., Equation B18).

A final useful form of the equations comes from eliminating $\dot{\theta}$ from equations B26 and B28 using equation B27. After some algebra and use of the relationship $\ddot{z} = v_z dv_z/dz = (1/2)d(v_z^2)/dz$ we get

$$\ddot{r} = r[(\omega_c/2)^2 - \Omega_c^2 (r_c/r)^4]$$

$$\dot{\theta} = \omega_c/2 - \Omega_c(r_c/r)^2$$

$$d(V_z^2)/dz = (e/m_0\gamma)(\Omega_c r_c^2 - \omega_c r^2/2)B_z'$$

where the cyclotron frequency, given by $\omega_c = eB_z/m_0\gamma$, carries the sign and the z dependence of the axial magnetic field B_z.

Note that equation B31 can be integrated to give

$$v_{z2}^2 - v_{z1}^2 = (e/m_0\gamma)[\Omega_c r_c^2 \int_{z1}^{z2} B_z dz - (1/2)\int_{z1}^{z2} \omega_c r^2 B_z' dz]$$

For the case of a stepped field (Equation B21) Equation B32 gives the following velocity change across the z = 0 boundary (assuming that $\theta = 0$ in Equation B25)

$$v_{z1}^2 - v_{z2}^2 = 1/4(e/m_0\gamma)^2 [r^2(o)(B_2^2 - B_1^2) - 2B_c r_c^2(B_2 - B_1)]$$

Here, r(o) is the radial position of the electron at z = 0. Note that the change in the z velocity depends on both the r_c and r(o). Thus, any spread in the radial positions of electrons at either the cathode source or at the position of the field step causes a corresponding spread in the z velocities of the electrons. This has important repercussions in gyrotron beam design.

APPENDIX C

DERIVATION OF ADIABATIC MIG DESIGN TRADE-OFF EQUATIONS

APPENDIX C

DERIVATION OF ADIABATIC MIG DESIGN TRADE-OFF EQUATIONS

In this Appendix we provide additional details on the derivation of the adiabatic MIG design trade-off equations given in Table I. For convenience we repeat this Table as Table CI in this appendix. These equations are written in a form to provide design values for eight gun quantities as a function of a single variable -- cathode radius, r_c. The remaining design constraints (parameters) are combined into a set of design constants designated as C_B, C_E, etc. The definitions of all variables are given in Part b of the Table in the order of their appearance in the Table.

Equation 1: $B_{zc} = C_B r_c^{-2}$

This equation is of such unique importance that its derivation has been covered separately in the previous Appendix B.

Equation 2: $E_c = C_E r_c^{-3}$

When a particle moves through a static magnetic field which varies slowly in space (compared to the dimensions associated with the cyclotron orbit), the flux linked by the particle's orbit remains constant. Therefore, Ba^2 is an adiabatic invariant where "a" is the radius of the cyclotron orbit in the magnetic field B.* This relationship is relativistically correct.

---

* J. D. Jackson, Classical Electrodynamics, John Wiley and Sons, New York, 1962, p. 582.

TABLE C-I(a)

Design Trade-off Equations for Adiabatic Gyrotron MIGs

1. $B_{zc} r_c^2 = B_o(b_o^2 - a_o^2)$ $\equiv C_B$

2. $E_c r_c^3 = \dfrac{\gamma_o v_{\perp o} C_B^{3/2}}{B_o^{1/2}\cos(\phi_c + \theta_B)}$ $\equiv C_E$

3. $d\, r_c^{-1} = \dfrac{\zeta a_o}{(b_o^2 - a_o^2)^{1/2}}$ $\equiv C_d$

4. $V_a r_c^2 = \dfrac{C_E \ln(1+C_d\cos\phi_c)}{\cos\phi_c}$ $\equiv C_V$

5. $\left(\dfrac{I_o}{I_L}\right) r_c^{-5} = \dfrac{2\pi J_c (1+C_d\cos\phi_c)\beta^2}{14.66(10^{-6})C_V^{3/2}\cos^2\phi_c}$ $\equiv C_L$

6. $\left(\dfrac{\Delta v_\perp}{v_\perp}\right)_T r_c^{-1} = \cdot \pm \left[\dfrac{C_B (kT_c/m_o)^{1/2}}{C_E \cos(\phi_c + \theta_B)}\right]$ $\equiv \pm C_T$

7. $\left(\dfrac{\Delta v_\perp}{v_\perp}\right)_R r_c^{1/2} = \pm\left[\dfrac{0.4\, C_B\sqrt{2\pi R}}{C_E^{1/2}\cos(\phi_c + \theta_B)}\right]$ $\equiv \pm C_R$

8a. $I_o r_c^{-2} = 2\pi\left(\dfrac{\ell_s}{r_c}\right) J_c$ $\equiv C_I$

8b. $\left(\dfrac{\ell_s}{r_c}\right) r_c^2 = \dfrac{I_o}{2\pi J_c}$ $\equiv C_\ell$

alternative equations

TABLE C-I(b)

Definition of Table Ia Variables (mks units)

r_c = Mean cathode radius

B_{zc} = Longitudinal magnetic field at the cathode

B_o = Magnetic field in rf interaction region

b_o = Final beam guiding center radius (central electrons)

a_o = Final cyclotron radius of electrons = $v_{\perp o}/\omega_c$

E_c = Surface electric field at midpoint of cathode

γ_o = Final beam relativistic mass ratio = m/m_o

$v_{\perp o}$ = Final beam transverse velocity

ϕ_c = Cathode angle with respect to axis (positive)

θ_B = Magnetic field angle WRT axis at cathode (negative for converging field)

d = Cathode-anode spacing measured normal to cathode

ζ = Number of Larmour radii across cathode-anode gap (can be adjusted for any desired anode voltage)

V_a = First anode voltage

I_o = Total beam current

(I_o/I_L) = Ratio of beam current to space-charge limited Langmuir current

J_c = Cathode surface current density

β^2 = Cylindrical diode geometry function (tabulated in Appendix C, Table CII). The argument of this function is $(1 + C_d \cos\phi_c)$.

$(\Delta v_\perp/v_\perp)_T$ = Standard deviation of transverse velocity spread in beam due to initial thermal velocities

kT_c/m_o = Boltzmann's constant x cathode temperature/electron mass

$(\Delta v_\perp/v_\perp)_R$ = Standard deviation of transverse velocity spread in beam due to cathode roughness

R = Characteristic roughness height of cathode (radius of hemispherical bump on cathode surface)

η = $|e|/m$ = charge to mass ratio of electrons.

(ℓ_s/r_c) = Ratio of slant length of cathode to mean radius

When the orbit radius is replaced by $a = v_\perp/\omega_c$ where $\omega_c = (e/m_0)B/\gamma$, the result is

$$\gamma^2 v_\perp^2/B = \text{constant of motion}$$

Equation 2 results from evaluating this constant at the cathode and in the rf interaction region and equating the two. Using $v_{\perp c} = E_c \sin\theta_{EB}/B_c$ and $\gamma_c = 1$, this gives

$$E_c = (B_c^{3/2}/\sin\theta_{EB})(\gamma v_{\perp o}/B_o^{1/2})$$

which can be put into final form using $B_c = C_B r_c^{-2}$ and $\theta_{EB} = \pi/2 - (\phi_c + \theta_B)$ where C_B, ϕ_c and θ_B are defined in table CI(b)

Equation 3: $d = C_d r_c$

The Larmour radius of electrons leaving the cathode is given by $a_c = v_{\perp c}/\omega_{cc}$. Using the definitions of $v_{\perp c}$ and ω_c given above, this gives

$$a_c = \gamma_c E_c \sin\theta_{EB}/\eta B_c^2$$

which upon elimination of E_c and B_c using equations 1 and 2 gives

$$a_c = a_o r_c/(b_o^2 - a_o^2)^{1/2}$$

Equation 3 results from the introduction of the arbitrary parameter $\zeta = d/a_c$ which gives the cathode-anode gap length in units of Larmour radius at the cathode. Since ζ is arbitrary, it can be used as a means for selecting the desired anode voltage since the constant C_d enters into equation 4.

Equation 4: $V_a = C_V r_c^{-2}$

This equation comes from cylindrical electrode theory. The radial electric field between two conducting coaxial cylinders of radii, r_1 and r_2 respectively ($r_2 > r_1 > 0$) is given by

$$E_r = V_0/r \ln (r_2/r_1)$$

where V_0 is the potential between the inner electrode and the outer electrode. If we replace r in the equation with $r_c' = r_c/\cos \phi_c$ and r_2/r_1 with $1 + (d/r_c)\cos \phi_c$ we get an equation which approximates the electric field at the surface of a cathode on the conical surface of an inner electrode with a similar conical surface a distance d away acting as the anode. (A drawing of this configuration is given in Figure C1). The resulting equation is

$$E_c = V_a \cos \phi_c/[r_c \ln (1 + d \cos \phi_c/r_c)]$$

The justification for this procedure is the fact that the curvature of a conical surface with respect to a plane passing through a line normal to the surface and perpendicular to the r - z plane, is given by the distance from the surface of the cone to the axis along the direction normal to the surface (r_c' in the figure C1.) The curvature of this surface along with the distance d across the gap to the anode of the voltage V_a gives a good approximation for the electric field at the surface of the cone when the distances involved are inserted into cylindrical electrode theory.

The derivation of equation 4 requires only the additional step of using equations 2 and 3 to eliminate E_c and d/r_c.

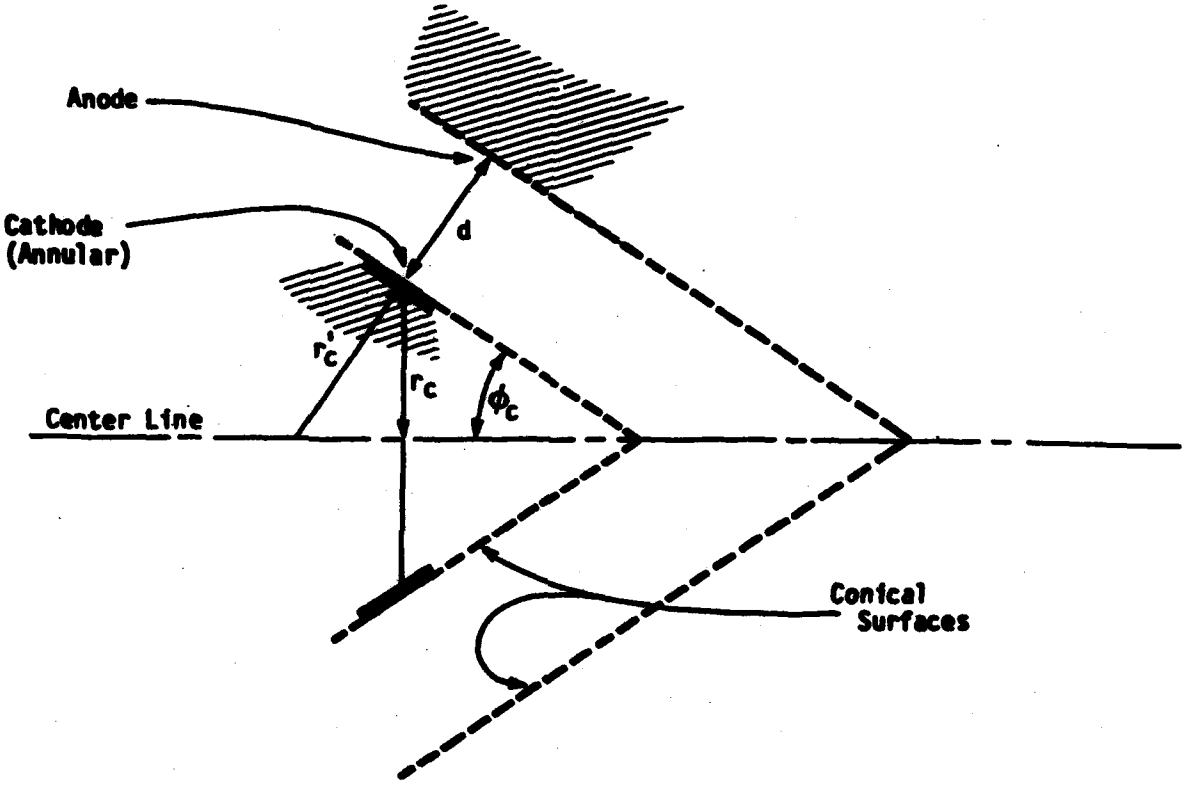

Figure C-1

Model for Effective Cathode Radius r_c' and Anode Spacing d
for MIGS with Large Cathode Angle Tilts ϕ_c

It is important to note that the asymptotic form of the cylindrical electrode equation for E_c as $\phi_c \rightarrow \pi/2$ is

$$E_c \rightarrow V_a/d$$

which is the field of planar diode with electrode separation d. Thus the equation appears valid for cathode angles from 0 to /2.

Equation 5: $(I_o/I_L) = C_L\, r_c^5$

To derive this equation for a conical electrode configuration it is necessary to make some assumptions about the limiting Langmuir current in the tilted cathode-anode geometry. When cathode tilt is zero, the cylindrical diode equations apply, and when cathode tilt is 90°, the planar diode equations must be used. As will be shown, the equations derived approach these two limiting forms.

We have assumed again that the radius of curvature at the cathode and the distance across the cathode gap are the determining factors of the space charge limited current. This seems justified on the basis that the virtual cathode which limits the current is formed very close to the cathode surface and is therefore primarily a function of the electric field which exists at the cathode in the absence of space-charge. It is also justified by the fact that a reasonable approximation to the potential across the cathode-anode gap can be obtained by replacing r_c in cyclindrical electrode theory by $r_c' = r_c/\cos\phi_c$. This has been verified by comparing the resulting potentials with those obtained by computer solution of LaPlace's equation in several MIG configurations. Accordingly, the Langmuir limited current for a tilted electrode system is obtained from the cyclindrical theory by simply replacing r_c with $r_c' = r_c/\cos\phi_c$.

The equation for the space charge limited current per unit length in a coaxial diode is given by*

$$J_L = 14.66(10^{-6})V_a^{3/2}/(r_a\beta^2)$$

where $r_a = r_c + d$ and $\beta^2 = \beta^2(r_a/r_c)$ is a geometry dependent function of r_a/r_c given in both series and tabulated forms in Table CII*. In the series expansion, the variable "ζ" is given by "ζ" = $\ell n\ (r_a/r_c)$. To put the cyclindrical and planar diode equations on a comparative basis we change J_L (amps/length) into J_L' (amps/area) by the relationship

$$J_L = J_L/(2\pi r_c)$$

We then replace r_c by r_c' to get

$$J_L' = 14.66(10^{-6})V_a^{3/2}\cos^2\phi_c/[2\pi r_c^2(1+d\ \cos\phi_c/r_c)\beta^2(1+d\ \cos\phi_c/r_c)]\ (amps/m^2)$$

If we compare this with the current density limit in a planar diode J_D

$$J_D = 2.334(10^{-6})\ V_a^{3/2}/d^2\ \ (amps/m^2)$$

we find that

$$\phi_c \longrightarrow \pi/2 \text{ limit } (J_L'/J_D) = 1$$

where we use the limiting form for $\epsilon << 1$

$$\ell_n^2(1+\ ) \simeq \epsilon^2$$

Thus, J_L' has the proper limiting forms for $\phi_c = 0$ and $\phi_c = \pi/2$, and we believe that it provides a reasonable measure of the limiting current for all angles in between.

---

* I. Langmuir and K. B. Blodgett, "Currents Limited by Space-Charge Between Coaxial Cyclinders", Physical Review Series 2, Vol. 22, pp 347-356, Oct 1923.

TABLE C-II

Evaluation of the function β^2 in the cylindrical diode equation.
(From Langmuir and Blodgett, 1923)

Coefficients of terms in series for β

(a)

$$\xi = \ln r/r_0$$
$$\beta = \Sigma A_n \xi^n$$
$$\beta = e^{-\xi/2} \Sigma B_n \xi^n$$

n	A_n	B_n
0	0.0	0.0
1	+1.0	+1.0
2	−0.40	+0.10
3	+ .09166667	+ .01666667
4	− .01424242	+ .002424242
5	+ .001679275	+ .0002872294
6	− .0001612219	+ .00002869476
7	+ .00001293486	+1.766121 × 10⁻⁶
8	−8.87693 × 10⁻⁷	+6.332946 × 10⁻⁸
9	+5.46192 × 10⁻⁸	−8.73852 × 10⁻¹⁰
10	−2.94843 × 10⁻⁹	−1.93844 × 10⁻¹¹
11	+1.36026 × 10⁻¹⁰	+5.77287 × 10⁻¹¹
12	−7.1101 × 10⁻¹²	+9.4502 × 10⁻¹³
13	+2.6644 × 10⁻¹³	+4.7012 × 10⁻¹⁴
14	+1.2526 × 10⁻¹⁴	−6.5539 × 10⁻¹⁶

β^2 as function of radius

r_0 = radius of cathode; r = radius at any point P
β^2 applies to case where P is outside cathode, $r > r_0$.
$(-\beta)^2$ applies to case where P is inside cathode, $r_0 > r$.

(b)

r/r_0 or r_0/r	β^2	$(-\beta)^2$	r/r_0 or r_0/r	β^2	$(-\beta)^2$
1.00	0.00000	0.00000	6.0	.8362	14.343
1.01	.00010	.00010	6.5	.8635	16.777
1.02	.00039	.00040	7.0	.8870	19.337
1.04	.00149	.00159	7.5	.9074	22.015
1.06	.00324	.00356	8.0	.9253	24.805
1.08	.00557	.00630	8.5	.9410	27.701
1.10	.00842	.00980	9.0	.9548	30.698
1.15	.01747	.02186	9.5	.9672	33.791
1.2	.02875	.03849	10.	.9782	36.976
1.3	.05589	.08504	12.	1.0122	50.559
1.4	.08672	.14856	14.	1.0352	65.352
1.5	.11934	.2282	16.	1.0513	81.203
1.6	.1525	.3233	18.	1.0630	97.997
1.7	.1854	.4332	20.	1.0715	115.64
1.8	.2177	.5572	30.	1.0908	214.42
1.9	.2491	.6947	40.	1.0946	327.01
2.0	.2793	.8454	50.	1.0936	450.23
2.1	.3083	1.0086	60.	1.0910	582.14
2.2	.3361	1.1840	70.	1.0878	721.43
2.3	.3626	1.3712	80.	1.0845	867.11
2.4	.3879	1.5697	90.	1.0813	1018.5
2.5	.4121	1.7792	100.	1.0782	1174.9
2.6	.4351	1.9995	120.	1.0726	1501.4
2.7	.4571	2.2301	140.	1.0677	1843.5
2.8	.4780	2.4708	160.	1.0634	2199.4
2.9	.4980	2.7214	180.	1.0596	2567.3
3.0	.5170	2.9814	200.	1.0562	2946.1
3.2	[illegible]	[illegible]	[illegible]	[illegible]	[illegible]
3.4	[illegible]	4.1126	[illegible]	1.0440	4973.0
3.6	[illegible]	[illegible]	[illegible]	[illegible]	[illegible]
3.8	[illegible]	[illegible]	[illegible]	[illegible]	7172.1
4.0	.6671	[illegible]	[illegible]	[illegible]	[illegible]
4.2	[illegible]	[illegible]	[illegible]	[illegible]	
4.4	[illegible]	[illegible]	[illegible]	[illegible]	
4.6	[illegible]	[illegible]	[illegible]	[illegible]	
4.8	[illegible]	[illegible]	[illegible]	[illegible]	
5.0	[illegible]	[illegible]	[illegible]	[illegible]	
5.2	[illegible]	[illegible]	[illegible]	[illegible]	
5.4	[illegible]	[illegible]	[illegible]	[illegible]	
5.6	[illegible]	[illegible]	[illegible]	[illegible]	
5.8	[illegible]	[illegible]	∞	[illegible]	∞

The final design relationship is obtained by taking the ratio

$$(I_0/I_L) = (J_c/J_L') = C_L r_c^5$$

where C_L is determined by using equations 3 and 4 to eliminate V_a and d from the equation.

Equation 6: $(\Delta v_\perp/v_\perp)_T = \pm C_T r_c$

This equation is derived utilizing the mean transverse thermal velocity at the cathode given by $\Delta v_{\perp c} = \pm (kT_c/m_0)^{1/2}$ and the adiabatic conservation of the transverse velocity spread $(\Delta v_\perp/v_\perp)$. This latter conservation theorem can be demonstrated by noting that for adiabatic beam flow, transverse velocities transform from magnetic field region 1 to magnetic field region 2 according to the relationship

$$\gamma_1 v_{\perp 1}/B_1^{1/2} = \gamma_2 v_{\perp 2}/B_2^{1/2}$$

If v is the only variable in this expression, then forming the ratio $\Delta v_\perp/v_\perp$ leads immediately to the result

$$(\Delta v_{\perp 1}/v_{\perp 1}) = (v_{\perp 2}/v_{\perp 2})$$

An estimate of the velocity spread in the final beam is therefore obtained by evaluating the spread at the cathode. The result

$$(\Delta v_\perp/v_\perp)_T = (kT_c/m_0)^{1/2}/(E_c \sin\theta_{EB}/B_c)$$

can be put into final form by using equations 1 and 2 to eliminate B_c and E_c respectively. We reiterate here that this trade-off equation only holds for

adiabatic flow through the acceleration region of the gun. Experience thus far with computer simulations shows that non-adiabatic effects can easily produce a factor of 50% error in the estimate. No physical measurements exist except as described in the Soviet work in Appendix A.

Equation 7: $(\Delta v_\perp / v_\perp)_R = \pm C_R r_c^{-1/2}$

The approach to the derivation of equation 7 is identical to that of equation 6 except that the transverse velocity at the cathode due to surface roughness is taken from an analysis by Tsimring (1972). Tsimring has analysed the velocity spread in electrons emitted from the surface of a small hemispherical bump of radius R on the surface of a planar cathode.
The result is

$$\Delta v_{\perp c} = 0.4\ (2\eta E_c R)^{1/2}$$

where $\eta = e/m_0$. Division of this equation by $v_{\perp c} = E_c \sin\theta_{EB}/B_c$ and elimination of E_c and B_c gives the trade-off equation shown as equation 7 in Table CI(a).

Equation 8: $I_0 = C_I r_c^2$ or $(\ell_s/r_c) = C_\ell r_c^{-2}$

These two expressions are simply alternative forms of the relationships between current I_0, current density j_c, and the slant length of the cathode ℓ_s:

$$I_0 = 2\pi r_c^2 (\ell_s/r_c) j_c$$

The slant length is normalized to the cathode radius as a convenience in design trade-off. Other forms of the expression can be used without effecting previously derived equations.